FUNDAMENTAL SCRATCH BEHAVIOR OF STYRENE-ACRYLONITRILE RANDOM COPOLYMERS

A Dissertation

by

ROBERT LEE BROWNING

Submitted to the Office of Graduate Studies of
Texas A&M University
in partial fulfillment of the requirements for the degree of

DOCTOR OF PHILOSOPHY

August 2010

Major Subject: Materials Science & Engineering

Fundamental Scratch Behavior of Styrene-Acrylonitrile Random Copolymers

FUNDAMENTAL SCRATCH BEHAVIOR OF STYRENE-ACRYLONITRILE RANDOM COPOLYMERS

A Dissertation

by

ROBERT LEE BROWNING

Submitted to the Office of Graduate Studies of
Texas A&M University
in partial fulfillment of the requirements for the degree of

DOCTOR OF PHILOSOPHY

Approved by:

Chair of Committee,	Hung-Jue Sue
Committee Members,	Zhengdong Cheng
	Andreas Holzenburg
	Chii-Der Suh
Chair of Materials Science and Engineering Program,	Ibrahim Karaman

August 2010

Major Subject: Materials Science & Engineering

ABSTRACT

Fundamental Scratch Behavior of Styrene-Acrylonitrile Random Copolymers.

(August 2010)

Robert Lee Browning, B.S., Texas A&M University;

M.S., Texas A&M University

Chair of Advisory Committee: Dr. Hung-Jue Sue

The present study employs a standardized progressive load scratch test (ASTM D7027/ISO 19252) to investigate the fundamental physical and mechanistic origins of scratch deformation in styrene-acrylonitrile (SAN) random copolymers. Previous findings from numerical simulation using finite element methods are used to establish correlation between mechanical properties and key scratch deformation mechanisms of the SAN model systems. For SAN, the acrylonitrile (AN) content and molecular weight (MW) can be changed to alter mechanical properties such as tensile strength and ductility.

The key scratch deformation mechanisms are identified as: scratch groove formation, scratch visibility, periodic micro-cracking and plowing. Groove formation has been correlated to the secant modulus at the compressive yield point while micro-cracking and plowing are related to the tensile strength of the material. The fundamentals and physical origins of scratch visibility are discussed. It is explained how unbiased evaluation is accomplished by means of an automatic digital image analysis

software package (ASV®). Frictional behavior and the effects of scratch speed and moisture absorption are also addressed.

Increasing the AN content and/or the MW of the SAN random copolymers generally enhances the scratch resistance of the material with regard to the onset of the key deformation mechanisms. Increasing the scratch speed increases the brittleness of the material, resulting in failure at lower applied loads. Moisture absorption increases with AN content and imparts a degree of plasticization as the moisture diffuses into the sub-surface. This plasticization initially results in a degradation of scratch resistance with respect to the key deformation mechanisms, but then, after saturation, the moisture on the surface provides lubrication and improves the scratch resistance. It is important to note that polymers are fundamentally different in nature, but the findings of this study serve as an important stepping stone down the path to a deeper understanding of polymer scratch behavior.

DEDICATION

To Dad and Meme

ACKNOWLEDGEMENTS

I would like to thank my committee chair, Dr. Sue, and my committee members, Dr. Cheng, Dr. Holzenburg, and Dr. Suh, for their guidance and support throughout the course of this research. I would also like to recognize the generous support from Rolf Minkwitz and Piyada Charoensirisomboon at BASF SE in Ludwigshafen, Germany and the Texas A&M Scratch Behavior of Polymers Consortium for the funding and material that made this work possible.

Next, I would like to sincerely thank my dad, Robert Browning. Without his guidance, wisdom and love, I would not have gone down the path that has led me to writing this dissertation. Thanks also to Kim, Meme (R.I.P.), Pawpaw, and my girlfriend, Dr. Sarah Pittman, DVM, whose undying support and love has been a morale booster throughout my studies. Thanks also to my friends and colleagues for making my time at Texas A&M University a great experience. I also want to extend my gratitude to Dr. Han Jiang, Allan Moyse, and Noah Smith, whose expertise has allowed the area of polymer scratch research to reach new and exciting levels.

Finally, I would like to sincerely thank the following for inspiration that got me through tough times: Bruce Lee, Phil Collins & Genesis, Buddy Rich, Neil Peart & Rush, Randy Rhoads, Brann Dailor, Allen Blickle, Spencer Seim, Chris Adler, Nintendo, Mega Man, Metroid, Zelda, Mario, Castlevania, Family Guy, Home Movies, Aqua Teen Hunger Force, King of the Hill, Metalocalypse, and too many others to mention.

TABLE OF CONTENTS

Page

LIST OF FIGURES

FIGURE Page

FIGURE Page

FIGURE Page

FIGURE Page

FIGURE Page

LIST OF TABLES

1. INTRODUCTION

This section serves to form a background for this dissertation by giving a brief description of the origins of standardized scratch testing and how scientific approaches have been employed to tackle the research. Factors and details motivating the current study will be presented and explained in detail. Finally, an overview of the components of the research and their arrangement in this dissertation will be given.

1.1 Origins of Scratch Testing

History shows that the beginnings of tribology can be traced back to Leonardo daVinci who conducted some of the first documented experiments on materials in relative sliding motion. A few centuries later, the first fundamental laws of friction were established by Charles-Augustin de Coulomb. Then, in 1812, Friedrich Mohs developed a mineral hardness scale based on the principle that a harder mineral can scratch a relatively softer one. In the centuries since its beginnings, tribology has expanded and grown into a multi-faceted field with great depth and a wealth of research possibilities.

The main concern of tribology centers on the study of wear, lubrication and friction. Wear can be observed as abrasion, adhesion, surface fatigue or tribologically-induced corrosion. When one considers the case of abrasion, two scenarios are possible:

This dissertation follows the style of Polymer.

1) Multi-pass where the sliding face encounters the face of the counterpart many times.
2) Single-pass where the sliding face encounters the face of the counterpart only once.

In the single-pass case, the face of the sliding component can exist as a collection of multiple asperities much smaller in size than the overall size of the sliding face (e.g. sandpaper) or it can exist as a "smooth" single asperity (e.g. a car key tip). The multi-asperity scenario will result in a collection of micro-scratches while the single-pass case will yield only a single scratch. This categorization is shown in Figure 1.1 in flowchart form as adapted from work by Professor Klaus Friedrich. The proposed work is concerned with applying the single pass/single scratch abrasion scenario in the wear category of the tribological field to polymeric materials. This path is denoted in Figure 1.1 with a red line.

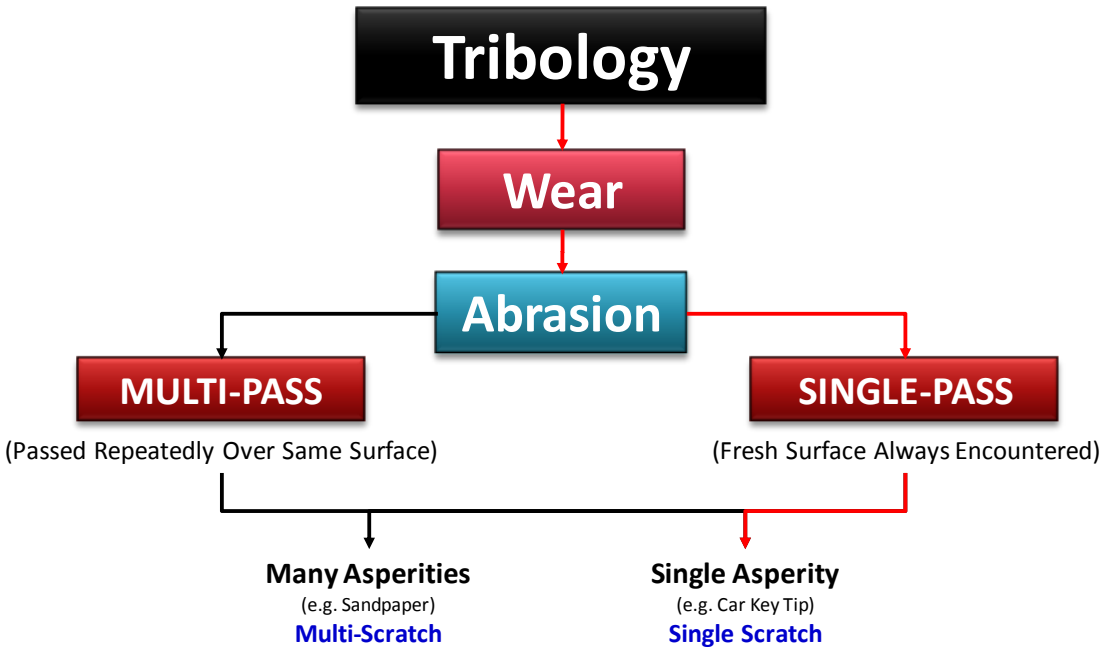

Figure 1.1 A flowchart characterization of the field of tribology.

In the past, a scratch has been envisioned as a sliding indentation, either under a constant or increasing load. Unfortunately, as is the case with most aspects of polymer science, this simplicity is quite deceiving. Addressing this issue is complicated due to the fact that polymers have complex material and mechanical behavior characteristics. Viscoelasticity, among other properties, plays a large role in the material response when a polymer is scratched. This creates a special challenge in developing test methods that address scratch behavior from a material science point of view. The challenge is augmented by the need to address the stress state the material experiences during a scratch. This is possible through numerical means (e. g. finite element methods), but the adopted model must be able to encompass the entire material response, i.e., linear elastic, anelastic, yielding, strain softening, and strain hardening. Also, and just as

importantly, quantitative evaluation of scratch resistance requires the elimination of ambiguity and subjectivity.

Often, scratch resistance is merely described with vague terms like “good” and “bad” or it is given a “pass” or “fail” designation. These terms do nothing to describe the nature of the material or why that particular material possesses “good” or “bad” scratch resistance. In studying polymer scratch behavior, there are three main areas of concern: aesthetics, structural integrity and durability. With regards to aestheticism, one can easily find its relevance in many products such as car dashboards and cellular phones where visible scratches reduce the original product’s superficial quality while the intended functionality remains. Poor durability means that surface scratches can lead to damage that compromises the lifetime of the component. This is especially important in transport applications where metal pipes are often coated with polymeric materials to prevent corrosion while exposed to the atmosphere or buried underground. In packaging applications, surface quality is extremely critical in upholding structural integrity. For example, in data storage, scratches on compact disks, hard disks and optical storage devices can cause permanent loss of data.

The main issue is how to link material properties to material performance with the purpose of differentiating materials with regards to scratch resistance. Diamond possesses the highest hardness of all materials and is thus impenetrable while an ideal rubber is soft and will recover completely if deformed. Therefore, in principle, these two materials possess the highest possible level of scratch resistance against surface deformation and damage upon removal of an applied load. Unfortunately, most

polymers lie in between and are extremely susceptible to scratch damage. As polymers have come to be relied upon more and more in a plethora of applications over the years, the demand for reliable scratch testing methods and objective analysis techniques has increased substantially. Until recently, no such testing method or analysis technique has existed.

Employing a reliable testing and analysis methodology that is founded upon the principles of material science and mechanics can make the objective understanding of polymer scratch behavior possible. Ideally, once the properties of the material are known and its behavior fairly well understood, numerical simulation employing mechanical modeling can be carried out to predict the outcome when a polymer is subjected to a particular testing scenario. Using the knowledge gained from these approaches, a deeper fundamental understanding of polymer scratch behavior can be achieved.

1.2 Research Motivations and Overview

Numerical methods make parametric studies on polymers considerably less complicated than experimental efforts. The reason is simply because numerical methods afford the advantage of being able to decouple the parameters of interest in a systematic fashion. In the real case, some properties like modulus and ductility are difficult to decouple. This makes it almost practically impossible to change one parameter while holding all others constant. Differences in crystallinity, the incorporation of additives and/or processing conditions can also add to the complexity of problem of trying to

identify a proper model system to perform an experimental parametric study. With the above issues of concern in mind, in order to experimentally carry out meaningful fundament study, a set of simple amorphous polymers has to be considered for this research.

The model system for this study is polystyrene-acrylonitrile (SAN) and is a random copolymer of polystyrene and polyacrylonitrile. Its repeat unit structure is given in Figure 1.2. Due to its higher strength and chemical resistance, SAN can be used as a commercial replacement for polystyrene. SAN is an amorphous copolymer typically composed of 20-35 wt% acrylonitrile (AN) and the remainder styrene. The amorphous nature of SAN is an attractive feature due to the inherent complex mechanical behavior of semi-crystalline polymers. In uni-axial tension, SAN has a ductility of approximately 2-3% and exhibits no signs of plastic yielding before breakage when tested under ASTM conditions (i.e., it is a nearly linearly elastic material). Its tensile properties (strength, ductility) can be controlled by changing the AN content [1]. All of these features point to the fact that SAN can be an ideal experimental model system for comparison to the numerical study.

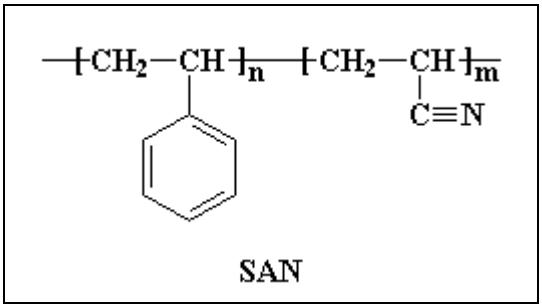

Figure 1.2 Repeat unit structure of polystyrene-acrylonitrile (SAN). In the grade proposed for this study, n and m are random.

Changing the AN content is one way to control the mechanical properties, but it is also known that changing the molecular weight can also alter the properties. Therefore, these factors inherent to SAN will be exploited in order to establish the link between material properties and scratch resistance.

Even though SAN has been identified as an ideal candidate for the fundamental study, there is one aspect of its material nature that requires consideration. The AN group of SAN consists of a nitrogen atom triple-bonded to a carbon atom and has a dipole moment of 3.9 DeBye, which is quite high. This means that the highly polar AN groups on the surface and immediate sub-surface of the SAN polymer can attract other polar molecules, namely water. Consequently, moisture in the atmosphere can be readily absorbed by the surface of SAN. Therefore, it is easy to see that addressing how the scratch behavior of SAN changes as a function of exposure to environmental moisture is a necessity.

In addition to addressing the scratch behavior of SAN from a fundamental standpoint, the fundamentals of scratch visibility in general will also be addressed. As

mentioned in the previous section, scratch visibility is of significant interest and requires objective and unbiased analysis. For many years, scratch visibility has been viewed as a highly qualitative performance criterion and its physical origins have not been very well understood. However, the identification of physiological parameters which govern how the average human eye perceives visibility has led to the development of an automatic scratch analysis software package which eliminates the element of human visual bias through the use of a desktop scanner. Additionally, there have been many recent advances in the understanding of surface/light interactions which has opened the door to understanding the physics of scratch visibility. The basic details of the software package will be explained and an example of its application will be shown by comparing the scratch visibility of polypropylene to polyvinylchloride.

To summarize the scope of this dissertation work, an overview of the research focuses is given in Figure 1.3.

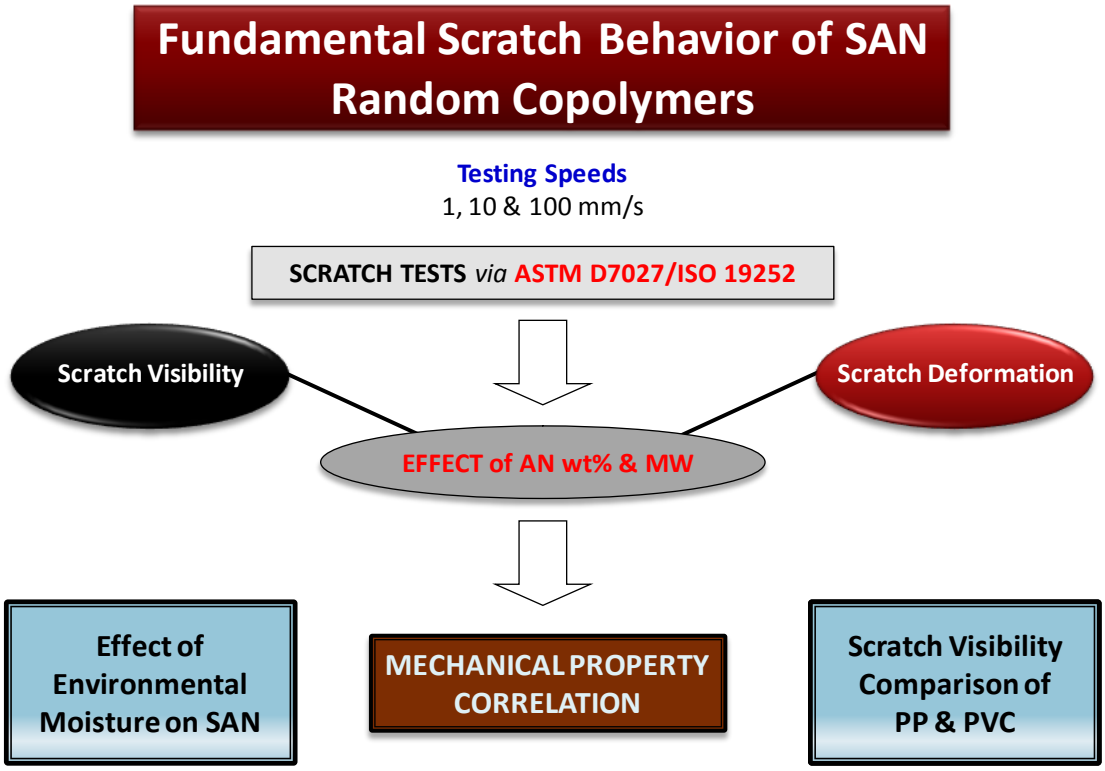

Figure 1.3 Overview of research focuses in the dissertation.

1.3 Layout of the Dissertation

To supplement the background presented in this section, a comprehensive literature review covering fundamental aspects of polymer scratch research and the basic mechanics of the scratch process will be given in Section 2. The standardized scratch testing methodology employed throughout this body of work will also be briefly described. In Section 3, the standardized methodology is applied to a set of SAN model systems with varying AN content at two levels of molecular weight. Key scratch deformation mechanisms for SAN are identified and will be described. The effects of testing speed and frictional behavior are addressed. Additionally, correlation with

mechanical properties will be established. Section 4 uses the same analyses as Section 3, but focuses on the change in MW at one level of AN content. The effect of exposure to environmental moisture on SAN scratch behavior is investigated in Section 5. Next, Section 6 covers the comparison of the scratch visibility of polypropylene and polyvinylchloride. It will be shown how the physical deformation resulting from the scratch process influences scratch visibility. Closing statements and considerations for future research efforts are given in Section 7. Finally, the citations of references in this dissertation will be documented.

2. LITERATURE REVIEW

Before any research endeavor of a fundamental nature can be undertaken, the current state of knowledge within the field must first be understood. This section presents a comprehensive literature review to explain the development of the testing methodology and to illustrate the work done by others in the field to gain fundamental understanding of polymer scratch behavior both from a mechanistic and aesthetic point of view.

Scratch research on metals and ceramics has been ongoing for quite some time, but polymer scratch research is still in its infancy. As polymers become more and more a material of choice for many engineering applications, the necessity for this type of research increases in turn.

Needless to say, numerous scratch testing methodologies been designed in recent years. Many efforts involved either using custom-made set ups or adapting existing machines to perform the task of putting a controlled scratch on a material surface. One common method was to use a nano-indenter or AFM and somehow change the function of the machine so that the tip can translate in a vertical direction as the indentation load is applied [2-11]. A meaningful study was conducted by Wong et al. who used a nano-indenter as a nano-scratcher to investigate the effects of crosslink density on the scratch of DER epoxy resins [11]. They found that increasing the crosslink density of the epoxy matrix increases the amount of elastic recovery after scratching and decreases penetration depth by the scratch tip. However, the tests were conducted at a constant

load, so there was no information gained as to load-dependent scratch-induced deformation mechanisms.

Since the tip employed by these nanoscale tests is so small, the applied load must be small as well to normalize the stress magnitude. The problem is that the geometry of the tips commonly employed in these devices is quite sharp and does not allow for a stress field evolution that is gradual enough to observe all of the scratch damage mechanisms of the material. Another issue with these methods is that the resulting scratches are so small that high-powered, expensive analysis instruments are needed to view the scratch. Real scratches can often be seen by the common observer without aid of such instrumentation. More powerful analysis instruments are only needed to view the deformation in high detail.

A comprehensive review of more practical devices is given by Wong et al. [12]. Among those test methods highlighted are the pencil test [13], the single-pass pendulum test [14, 15], the pin-on-disc test [16], the Revetest scratch device [17], the Taber scratcher [2] and the Ford Five-Finger scratch tester [18, 19]. Even though these methods can produce scratches in a repeatable manner, there are still factors that affect their reliability.

Literature on polymer scratch testing can be found dating back to 1955 where modified polystyrenes were explored as a material for telephone housings [20]. Numerous other studies have since been conducted over the years, but scientific depth is generally lacking [11,12,19,21 - 59]. Then, the continuous research efforts at Texas A&M involving polymer scratch behavior resulted in the development of a progressive

load scratch testing methodology that has been standardized under the designations ASTM D7027 (est. 2005) and ISO 19252 (est. 2008) [60, 61]. The progressive load nature of this scratch test allows one to directly link the applied normal load to the onset of any damage feature along the scratch path by measuring the scratch distance.

The scratch testing apparatus shown in Figure 2.1, the Scratch 4 Surface Testing System, was designed by Surface Machine Systems (www.surfacemachines.com) in conjunction with the Polymer Technology Center at Texas A&M. It is equipped with normal and tangential load sensors so that the frictional force throughout the scratch can be measured. The main advantage of the progressive load test is that it shows a continuous evolution of the scratch damage in a single pass. The research carried out using the ASTM/ISO scratch test suggests that the methodology has significant scientific merit [12,28,29,57,59, 62 - 69].

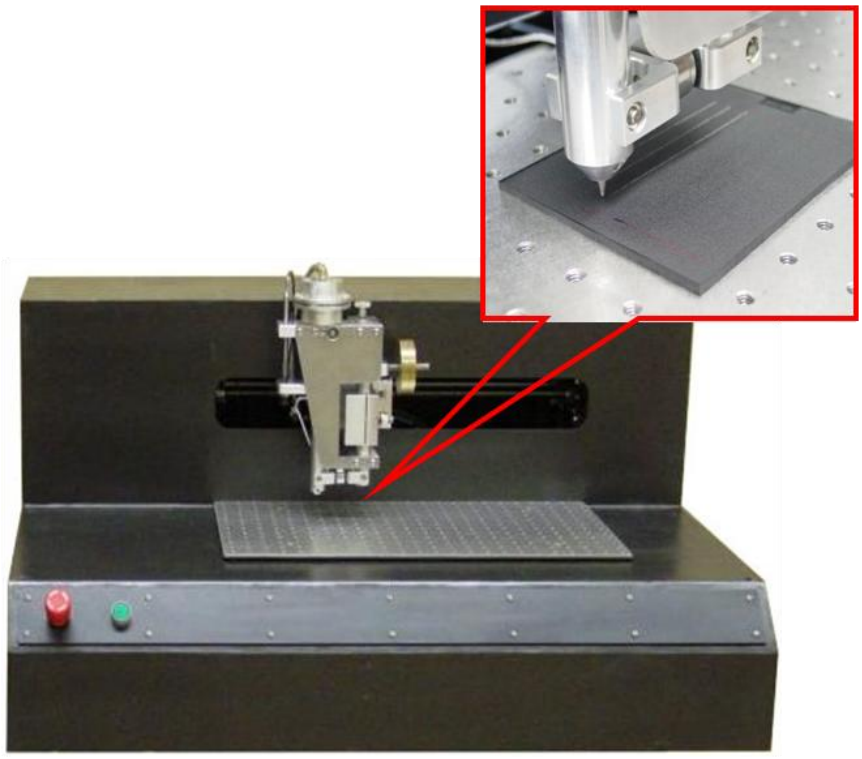

Figure 2.1 The Scratch 4 Surface Testing System designed by Surface Machine Systems and the Polymer Technology Center at Texas A&M University.

The evaluation of scratch resistance must be founded on the fundamental principles of material science. Intuitively, the scratch-induced deformation is strongly related to the stress and strain the material experiences during the scratch process. In general, the scratch process involves a normal load applied to an asperity while in a sliding motion (see Figure 2.2). This results in the application of multi-axial stress of compressive and tensile nature, as shown in Figure 2.3 [70].

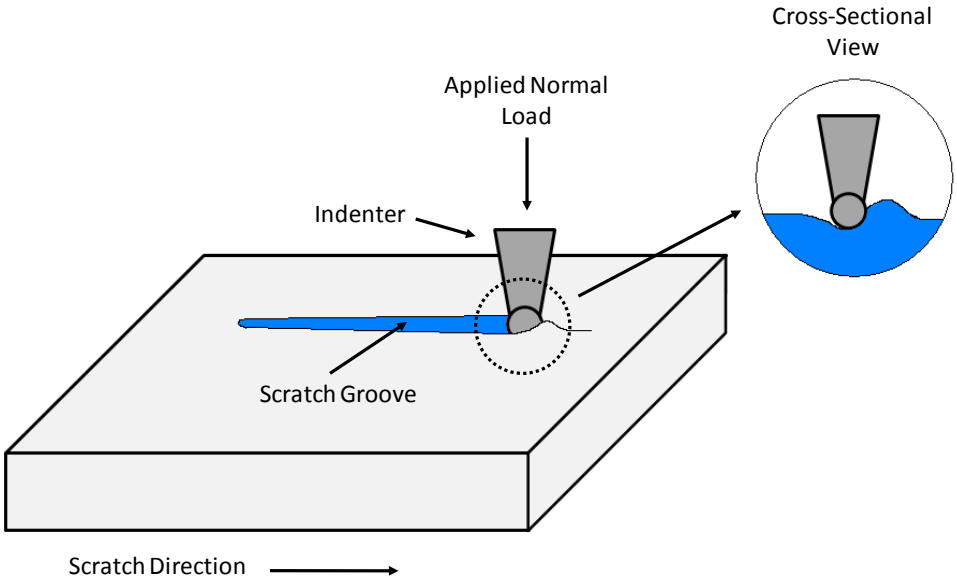

Figure 2.2 Schematic illustration of the scratch process.

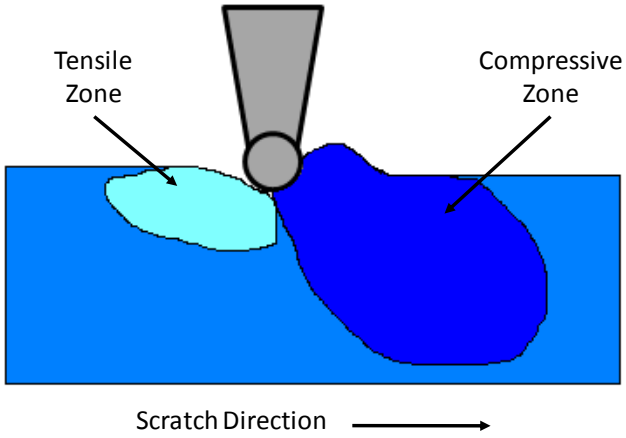

Figure 2.3 Illustration of stress zones present during the scratch process.

Measuring the mechanical properties of a material is often a good way to gauge its performance in certain applications. However, the multi-axial nature of the scratch stress field presents a challenge when attempting to relate the mechanical properties to

the resulting scratch deformation. Furthermore, there are several properties unique to polymers like viscoelasticity and differences in molecular architecture that make the situation even more complicated.

Numerous researchers have tried novel ways of relating scratch behavior to material properties. Xiang, et al. conducted a study on the relationship between polymer scratch deformation phenomena and mechanical properties based on a variety of amorphous and semi-crystalline polymers [59]. In particular, the surface tensile stresses were used to gauge the scratch resistance of the polymers with respect to onset of plastic flow or brittle surface fracture. However, no detailed knowledge was gained in addressing correlation between the material properties and scratch damage mechanisms.

Since polymers are viscoelastic materials, their deformation behavior depends on the temperature and rate at which the tests are performed. Jardret and Morel studied the effects of temperature and strain rate on the scratch deformation of PMMA [70]. Their study found that as the temperature increases, the material around the scratch tip is deformed quite easily and also that if the scratch speed is increased, the brittleness of the material increases and fracture occurs earlier. A similar study was carried out by Browning, et al. to investigate the effect of scratch speed on the scratch behavior of soft TPOs [62]. The findings were similar in that, even though the TPOs were soft and rubbery, the material behaved in a more rigid and brittle fashion at higher testing speeds.

Surface friction is a complicated concept, but is vital to consider when studying scratch behavior. There have been numerous efforts to link surface friction with polymer scratch behavior [38, 63, 64, 71 - 74]. Pelletier et al. investigated the effect of

the friction coefficient on the resulting contact area during scratching indenter of amorphous polymers with a spherical using experimental efforts coupled with numerical simulation [74]. Their detailed study concluded that the local coefficient of friction has an impact on the maximum value of equivalent strain and can affect the shape of the plastically deformed volume. Browning et al. looked at the effect of incorporating erucamide, a slip agent, into talc-reinforced TPOs and found that increased lubrication of the surface led to significantly improved resistance to scratch visibility [38]. Furthermore, Jiang et al. probed the effects of surface roughness on frictional behavior and its relationship to scratch behavior [64]. Their findings show that if the surface roughness increases, the friction during scratching is reduced, leading to improved scratch resistance.

One way many researchers have attempted to enhance the mechanical properties of polymers is by adding nanoscale fillers to make polymer nanocomposites. Indeed, the mechanical properties of polymer nanocomposites were greatly improved over those of the neat systems and studies in polymer nanocomposite scratch behavior followed suit [47, 69, 75 - 77]. In a study on nanoclay-reinforced PP and PE, Yuan et al. found that incorporation of the nanocomposites decreased the susceptibility of the systems to micro- and nano-scale deformation in the form of surface ripples [76]. They attributed this improvement to increases in crystallinity, elastic recovery, modulus and yield strength. In a comprehensive review of nanocomposite scratch, Dasari et al. point out that incorporation of nanofillers does not always bring improvements [77]. This was also shown in work carried out by Moghbelli et al. on epoxy nanocomposites [69]. The

incorporation of α-Zirconium Phosphate or core-shell rubber particles into epoxy matrices was found to improve the mechanical properties, but the resistance scratch-induced surface deformation was actually lower. This method of improving mechanical properties is not very sound because incorporation of fillers into a polymer matrix alters its physical nature and limits the understanding of the impact of microstructural parameters on tribological behavior. A more practical way of changing the mechanical properties of a polymer is by changing the molecular weight. Increasing the molecular weight generally increases the tensile strength and ductility and has been linked to enhanced scratch resistance in material like PP, HDPE and UHMWPE [26, 29, 40, 68, 78 - 84].

When characterizing the mechanical behavior of polymers, it is important that the characterization be general and comprehensive. The important idea of polymer scratch maps came from Briscoe, et al. in 1996 [26, 29]. Their studies involved such approaches as relating hardness and the scratch-induced strain to the surface deformation of PE, PC and PMMA and under what level of applied normal load the deformation occurred. In a similar fashion, Sue and co-workers developed a scratch map for polymers based on the strength and ductility of several polymers and how it relates to the resulting scratch deformation features [65]. These maps provided generalized information regarding scratch damage as a function of several scratch testing and material parameters like testing speed, modulus, ductility, etc.

Evaluation of scratch resistance is sometimes approached from an aesthetic view. Visible scratches can degrade the visual quality of polymer surfaces. Scratch visibility

has long been thought to be a qualitative phenomenon in that human perception is often depended upon for assessment. However, many people have made attempts at objectively approaching the issue [2, 12, 67, 85, 86]. By using setups comprised of controlled illumination and detectors, insight can be gained as to how incident light interacts with a scratched surface [27]. However, only marginal understanding is gained regarding the root cause of scratch visibility as it relates to surface deformation.

3. OBJECTIVE SCRATCH VISIBILITY ASSESSMENT

Scratch visibility can be immediately appreciated by anyone concerned with aesthetic surface quality. However, until recently, the analysis methodologies used to assess scratch visibility have been highly qualitative and subjective. Human bias, surface/light interactions (i.e. orientation of the scratch with respect to the illumination source) and how the physics of surface deformation relates to scratch visibility are all key elements to developing objective analysis methodologies. This section will describe a software package called ASV® that has been developed to automatically analyze scratch visibility using human physiological parameters. Polyvinylchloride (PVC) has long been considered to exhibit extremely "good" scratch resistance compared to other polymers like polypropylene (PP). Therefore, the scratch visibility resistance of homopolymer PP and rigid PVC will be utilized as a set of model systems to illustrate how scratch visibility is assessed by the ASV® software. Details regarding the operating principles of the software and the relationship between surface deformation and scratch visibility will be discussed.

3.1 Details of Scratch Visibility Analysis Software

A surface scratch will only be visible once the contrast between the scratch damage and the background reaches a certain level. For the typical human eye, this level is 3% for matte surfaces and 2% for glossy surfaces. Additionally, the smallest feature size the human eye can resolve as a single entity is roughly 90 μm. These parameters

are used in conjunction with the commercially available software package ASV® to automatically analyze a digital image of a scratched sample and detect the onset of scratch visibility based on the contrast and size criteria mentioned above.

For quantitative scratch visibility resistance evaluation, a sample is scratch tested according to the ASTM/ISO standard methodologies. Then, the surface of the sample is scanned using a PC-based scanner at a resolution of 300 dpi (i.e. 90 μm/pixel). A Munsell mini colorchecker is scanned simultaneously with the sample to allow for color calibration in the ASV® software. Once the digital image is obtained, the algorithm in the software scans the image to locate the point at which the contrast and feature size criteria are met. Furthermore, a continuity criteria has been introduced to account for the stick-slip phenomenon and the presence of artificial features like dust particles, bumps, surface texture, etc. that could affect visibility assessment. When all the criteria are simultaneously met, the software scans the corresponding data file from the executed scratch test and reports the Critical Load for the Onset of Scratch Visiblity. The critical load can then be used as an objective metric to rate scratch visibility resistance. A more detailed description of the ASV® software can be found in [67] or at http://www.surfacemachines.com.

3.2 Model PP and PVC Systems

Injection-molded homopolymer PP and rigid PVC plaques in the dimensions of 170 mm by 110 mm by 3 mm were used for this study. All samples had smooth, flat surfaces, i.e., RMS virgin roughness = ~83 nm. Although the PVC formulation is

proprietary, it was provided that the rigid PVC formulation contained stabilizers and processing additives like paraffin wax and plasticizer. Carbon black pigmentation was added for contrast purposes. To compare the scratch behavior of PP and PVC, the mechanical properties should be as similar as possible. The flexural modulus was matched for the two materials and was given as 2.2 GPa. The corresponding flexural strength was 57 MPa for PP and 74 MPa for PVC.

3.3 Scratch Testing and Analysis

Scratch tests were performed following the ASTM D7027-05 standard. In this case, a progressive load ranging from 1 – 90 N was applied to the PP and PVC. Four tests were conducted for each material at a rate of 100 mm/s for a length of 100 mm.

Upon completion of the tests, the samples were stored at ambient temperature for at least 72 hrs to allow for viscoelastic recovery of deformed region to stabilize. Then, the scratched samples of PP and PVC were scanned simultaneously with a Munsell color checker using an EPSON Perfection 4870 Photo PC scanner at a resolution of 300 dpi. To analyze the effect of observation angle, two scan orientations were employed: one where the scanning direction was parallel to the scratch testing direction and the other where the scanning direction was perpendicular.

After obtaining the digital images, the ASV® software was used to normalize the images using the standardized values of red, blue and green on the color checker. This step is to ensure that the digital image represents as closely as possible what a human observer would see with un-aided eyes. The Critical Load for the Onset of Visibility

was then obtained using the physiological criteria of 3% contrast, 90 μm feature size and 90% continuity.

To relate the visibility of the PP and PVC samples to the corresponding scratch damage morphology, a Keyence VK-9700 violet laser scanning confocal microscope (VLSCM) was used to obtain cross-section profiles for topology measurement and values of RMS surface roughness at increments of 10 mm along the scratch path. For the roughness measurement, the parabolic profile of the cross-section was flattened using tilt-correction options within the Keyence VK Analyzer software. RMS roughness values were obtained using a circular measurement window with a diameter of 270 μm.

3.4 Results and Discussion

3.4.1 Scratch Damage Observation

Figure 3.1 shows the scanned images of the tested samples. It can clearly be seen that, regardless of scan orientation, PVC has a superior scratch performance in that the onset of visibility is significantly delayed. Figure 3.1 also shows that for some materials, the observation angle can be a critical factor when assessing scratch performance. PP shows little if any dependence on scan orientation while the difference for PVC is quite substantial.

The plowing point is where the stress applied by the scratch tip reaches the strength of the material. The tip penetrates through the surface and begins to displace the material in front of and around it. When considering this scratch damage feature,

PVC also clearly shows superiority over PP. A summary of the critical load values for orientation-dependent visibility and the onset of plowing is given in Figure 3.2.

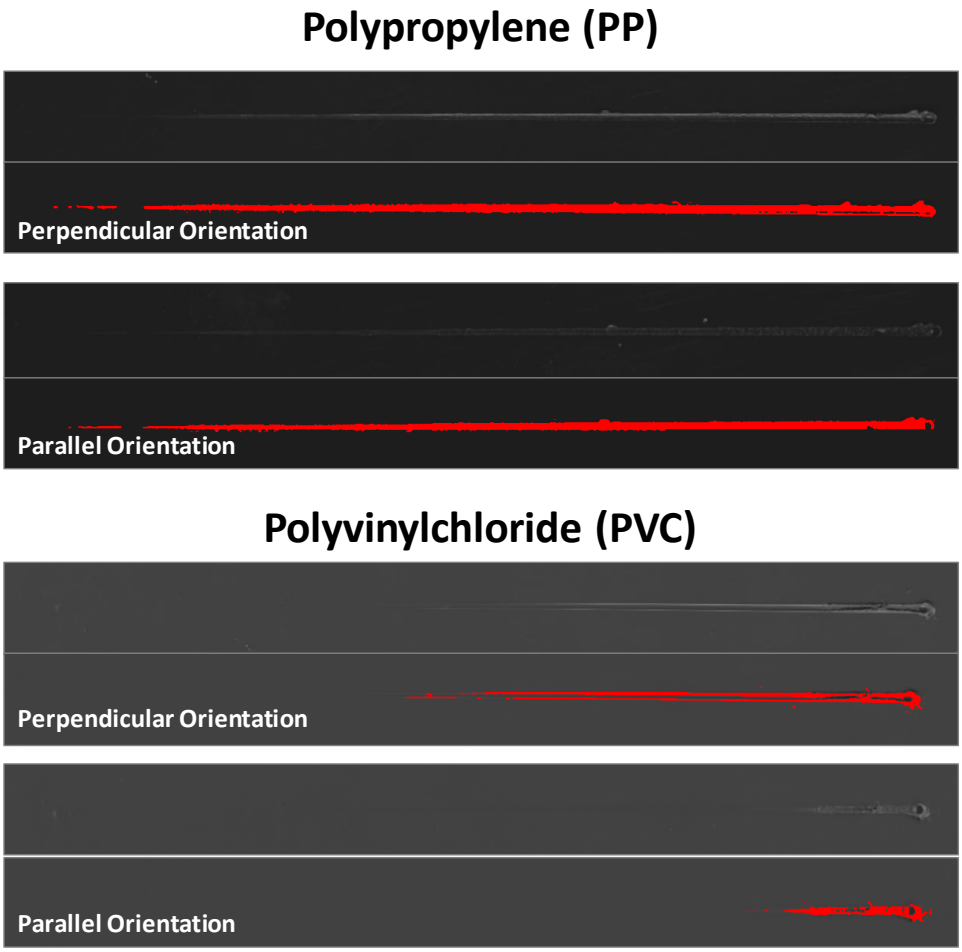

Figure 3.1 Scanned images of scratched samples of model PP and PVC. (Resolution = 300 dpi)

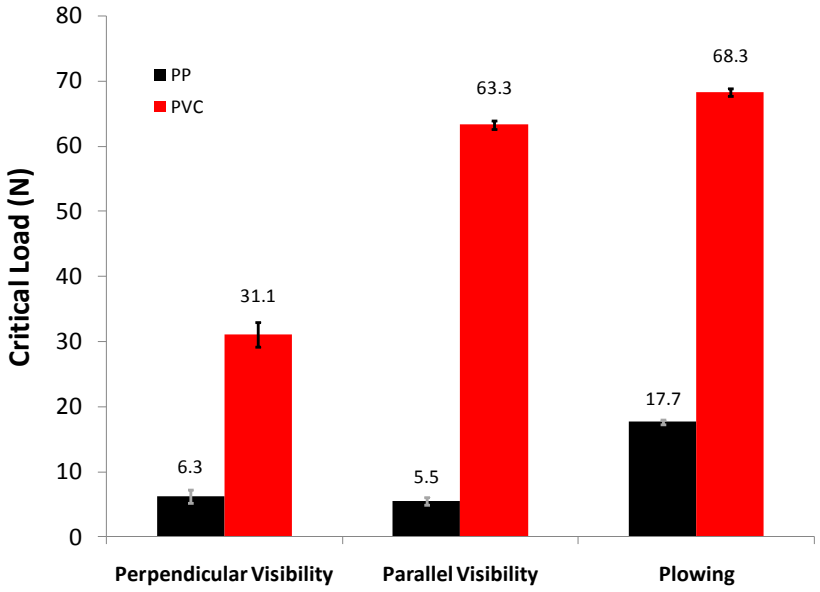

Figure 3.2 Summary of critical load values for visibility and plowing for model PP and PVC.

3.4.2 Relating Scratch Visibility & Surface Characteristics

As stated earlier, the two main morphological factors affecting scratch visibility are surface roughness and the topology of the scratch profile. If the scratch is illuminated with the incident angle perpendicular to the scratch, the topology will be the dominant factor. However, if the angle of incidence is parallel, the scratch will be illuminated in a more uniform manner and the surface roughness will play the most important role to trigger visibility. A detailed illustration is shown in Figure 3.3.

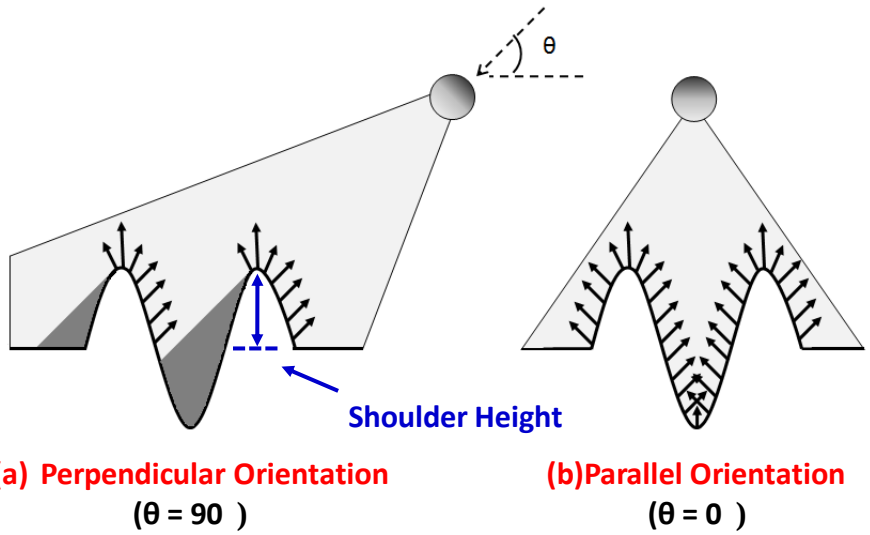

Figure 3.3 Illustration of factors affecting surface/light interaction: a) Profile/geometry change in perpendicular scanning orientation and b) surface roughness change in parallel scanning orientation.

As the applied load increases, the topology of the scratch profile changes in turn. The plastic deformation from the scratch process results in a shoring-up of material on the sides of the scratch. The height of the shored-up material, or shoulder height, will eventually increase to a point where the angle of reflection will be altered to create a shadow with an intensity level different high enough to introduce at least 3% contrast relative to the background (see Figure 3.3a). In the other scenario, as shown in Figure 3.3b, the surface roughness must increase to a high enough level so that the scattered light intensity is high enough to meet the 3% contrast criterion.

Figures 3.4 and 3.5 shows shoulder height and RMS roughness as a function of applied normal load for the model PP and PVC systems. The gray dots lying on the

curves represent the visibility points for PVC and PP as related to that feature. The shaded boxes indicate that plowing has occurred for that material.

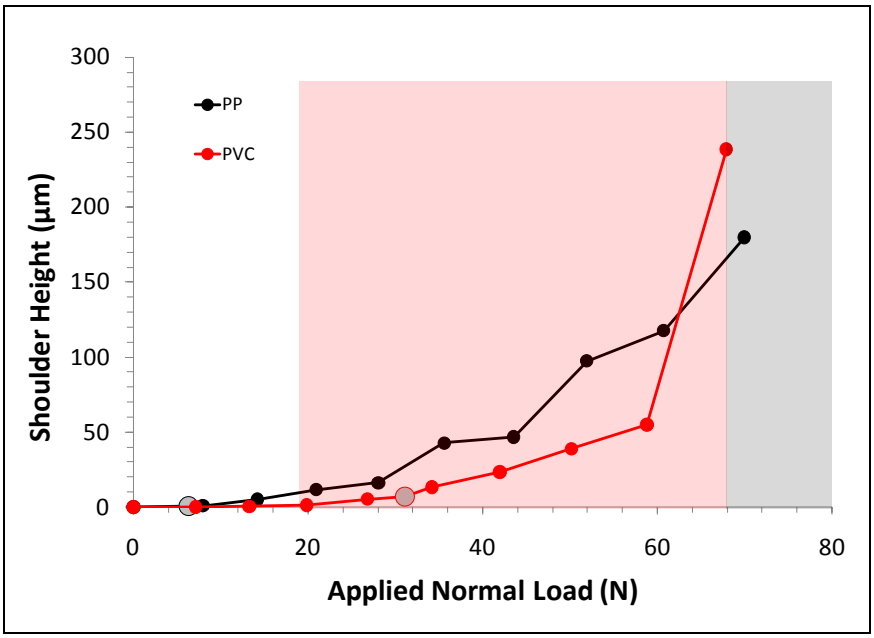

Figure 3.4 Shoulder height as a function of applied normal load for model PP and PVC.

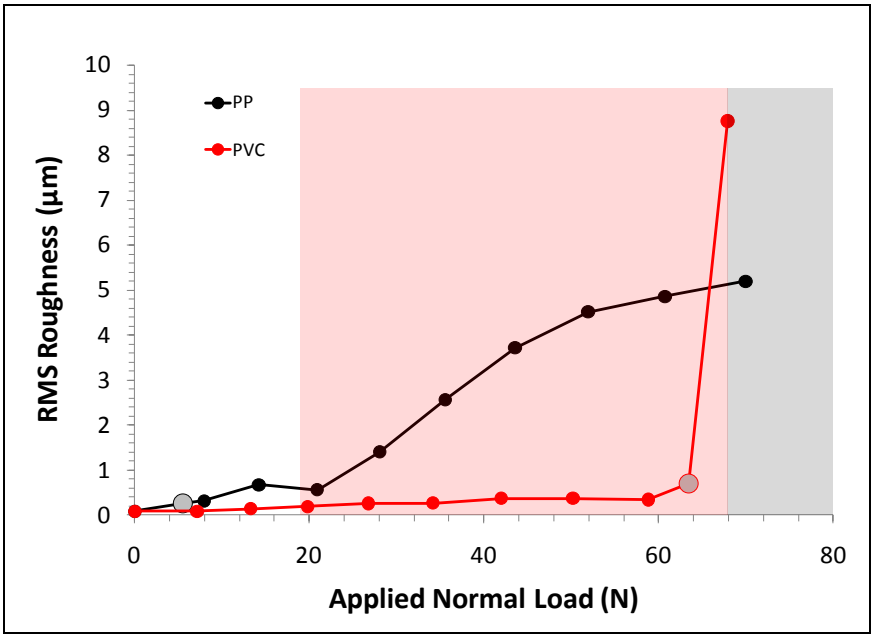

Figure 3.5 RMS surface roughness as a function of applied normal load for model PP and PVC.

Figure 3.4 shows that the shoulder height of PVC evolves much more gradually while for PP, the topology change is almost instant. The same can be said for the roughness (see Figure 3.5). PVC maintains a smooth scratch profile until just about the plowing point while PP roughens almost instantaneously. In Figure 3.6, the close-up scans of the region around the plowing point make it readily apparent that PVC maintains a smooth profile until just before plowing.

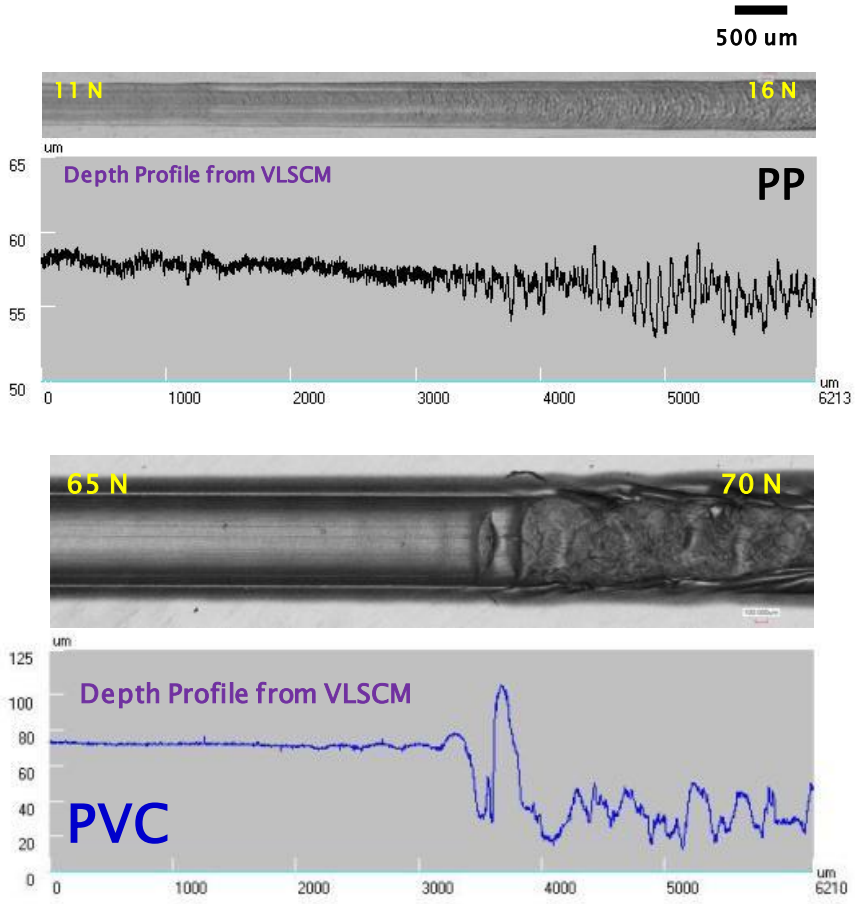

Figure 3.6 VLSCM scans of PP and PVC just before the plowing point.

It is well known in the field of tribology that improving the frictional behavior of a polymer can result in an improvement in resistance against surface deformation and damage [63]. The ratio of the tangential and normal loads throughout the scratch is termed the scratch coefficient of friction (SCOF) and is shown for the two model systems in Figure 3.7.

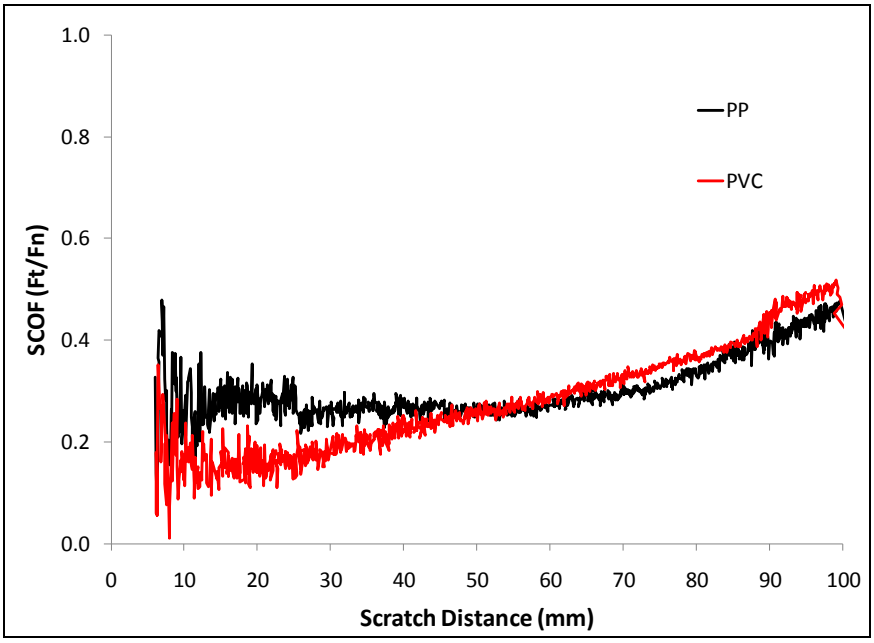

Figure 3.7 SCOF as a function of scratch distance for model PP and PVC systems.

Up until about a scratch length of 50 mm, PVC intuitively exhibits lower frictional behavior, but then continues to increase with increasing load. This is likely because of the fact that as the tip continues to penetrate, more material is present in front of the tip which gives rise to a new component of the tangential force related to material resistivity. As for PP, it is likely that the debris formed a transfer film layer with the indenter during scratching, which helped to stabilize the SCOF even when a higher scratching load is applied.

It was originally thought that the higher strength of PVC was the cause of the superior scratch resistance. While it is true that PVC is more resistant than PP to plastic deformation (i.e. groove and shoulder height formation), it was realized after observing

the roughness and friction behavior that some of the waxy additives, necessary for commercial production, could be artificially improving the scratch resistance.

In conclusion, the value of the ASV® software as a quantitative scratch visibility analysis tool is definitively showcased by the findings of this study. As such, the SAN model systems will be analyzed in the same way as the PP and PVC to understand how the incurred surface deformation influences the resulting scratch visibility behavior.

4. EFFECT OF ACRYLONITRILE CONTENT ON SCRATCH BEHAVIOR OF SAN MODEL SYSTEMS

This section introduces the application of the progressive load methodology from the ASTM/ISO standard to a set of model SAN systems with varying AN content at two levels of molecular weight (MW). The scratch behavior is analyzed in detail and key damage mechanisms are identified. Using the knowledge of the basics of scratch mechanics, correlations between scratch deformation and mechanical properties are established. Scratch visibility, rate dependence and frictional behavior are analyzed, as well.

4.1 Model SAN Systems

The SAN systems for this study were provided by BASF SE with varying level of AN content in the form of reactor-grade random copolymers polymerized by free-radical reactions. Two grades of SAN containing 27 wt% AN and differing MW were employed for the study so that the effect of AN content and MW could be de-coupled. In that regard, the comparisons made in this study will focus on the AN content effect at two levels of MW. The MW effect at a constant level of AN content will be addressed in the next section.

The resins were produced into injection-molded plaques with dimensions of 150 mm by 150 mm with a thickness of 6 mm. The surface finish of the plates was smooth with a 60° specular gloss of 95. Upon receipt, the injection-molded plaques were

annealed between two smooth glass plates at 110 °C for 2 hours to relax residual surface stresses resulting from the injection molding process. It was verified through profilometry with a laser confocal microscope that the surface finish was not affected by the annealing process. To create a sufficiently dark-colored material for scratch visibility analysis purposes, 0.325% of anthrachinone and 0.15% of pyrazolone yellow were incorporated into the resins.

Physical properties of the model systems were evaluated by BASF SE and are summarized in Table 4.1. The MW was obtained from light scattering measurements and polydispersity is defined as M_w/M_n. Poisson's ratio for all SAN systems was assumed to be 0.35 as quoted in the literature [87].

Table 4.1 Physical properties of SAN model systems for the AN content effect study

	SAN19	**SAN27** (Hi MW)	**SAN27** (Lo MW)	**SAN35**
Acrylontrile Content (wt%)	19	27	27	35
Molecular Weight (kg/mol)	134	134	106	104
Polydispersity	4.1	4.4	3.9	3.7
Poisson's Ratio	0.35	0.35	0.35	0.35

4.2 Experimental Procedures

Tensile and compression tests were performed on a screw-driven MTS® Insight load frame equipped with a 30 kN capacity load cell. MTS® Testworks 4 was used as the software interface for data collection.

For uni-axial tensile testing, injection-molded dog-bone specimens of the model systems were prepared by BASF SE with a nominal thickness and width of 4 mm and 10 mm, respectively. Actual dimensions were measured with a digital micrometer caliper. The crosshead speed for the tensile tests was 5 mm/min and an MTS® extensometer with a gauge length of 25.4 mm was used to monitor the displacement for strain calculations.

Uni-axial and plane-strain compression specimens were prepared from the 6 mm thick injection molded plates by precision-cutting using a diamond saw. The nominal dimensions of the compression specimens were 12.7 mm by 6 mm by 6 mm for uni-axial compression and 12.7 by 12.7 by 6 mm for plane-strain compression. After the samples were cut with the diamond saw, the faces were polished using first P2400 and then P4000 grit silicone-carbide abrasive paper. Care was taken to ensure that all edges were flat, square and parallel. Actual dimensions of the specimens were measured using a digital micrometer caliper.

Uni-axial compression tests were performed using a parallel-plate setup while plane-strain compression tests involved a channel - die configuration similar to that employed by Boyce, et al. [88]. Both the width of the channel and the thickness of the die were 6 mm. The other dimensions were configured to allow ample space for deformation after the onset of plastic flow. A setup consisting of linear bearings and guide rods was used to ensure proper alignment for both compression scenarios. A crosshead speed of 2.5 mm/min was chosen so that the strain rate in compression was equal to the strain rate in tension. The MTS® extensometer was applied to each fixture

to monitor displacement for strain calculations. White lithium grease was used to provide sufficient lubrication and minimize friction under compression.

Scratch tests were carried out according to the conditions outlined in ASTM D7027-05/ISO 19252:08 by using a progressive load range of 1 – 90 N at constant scratch speeds of 1, 10 and 100 mm/s for a length of 100 mm. The scratch tip was made of stainless steel in a spherical geometry with a diameter of 1 mm. Three scratch tests were performed at each speed on the same SAN plaque. All tests were performed so that the tip movement was the same as the melt flow direction.

A Keyence® VK9700 violet laser scanning confocal microscope (VLSCM) was used for high-resolution analysis of the surface roughness and scratch damage mechanisms. The samples were analyzed 48 hrs after the completion of scratch tests. The microscope is equipped with a 408 nm wavelength violet laser and has an x-y-axis resolution of ~250 nm while the height resolution is ~1 nm. The VK Analyzer software provided with the microscope was used to obtain optical images as well as topographical profiles. The tilt-correction and noise-filtering capabilities available in the software were used to process the raw images. RMS surface roughness was also measured using the VK Analyzer software. To measure the roughness of the scratch path, the hemi-spherical profile was flattened using a curve-fitting option in the VK Analyzer software. The window for roughness measurement was circular with a diameter of 270 μm to correspond with the physiological resolution criterion of the human eye (smallest resolvable feature size = 90 μm).

An Olympus® BX60 optical microscope was used in reflection mode when high-resolution damage analysis was not required.

4.3 Results and Discussion

4.3.1 Mechanical Properties of Model Systems

The stress-strain curves for the model SAN systems under uni-axial tension are shown in Figure 4.1. Under compression, the only appreciable difference observed between the uni-axial and plane-strain compression stress-strain curves is the strain-hardening exponent. Therefore, typical compressive stress-strain curves for the SAN systems are shown in Figure 4.2. The tensile and compressive properties are summarized in Tables 4.2 and 4.3.

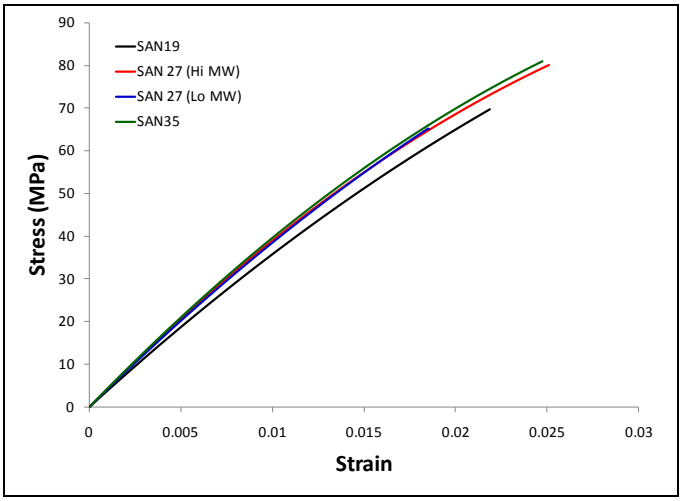

Figure 4.1 Stress-strain curves for model SAN systems with varying AN content under uni-axial tension.

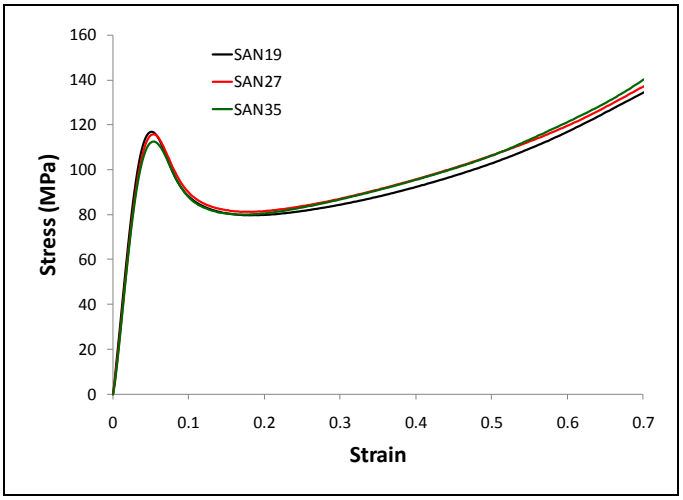

Figure 4.2 Typical compressive stress-strain curves for model SAN systems with varying AN content.

Table 4.2 Uni-axial tensile properties of SAN model systems for the AN content effect study

	SAN19	**SAN27** (Hi MW)	**SAN27** (Lo MW)	**SAN35**
Modulus (GPa)	3.4 ± *0.04*	3.7 ± *0.11*	3.5 ± *0.09*	3.7 ± *0.02*
Tensile Strength (MPa)	68.9 ± *1.5*	79.0 ± *1.0*	59.3 ± *2.7*	81.9 ± *0.7*
Ductility (%)	2.20 ± *0.07*	2.57 ± *0.04*	1.68 ± *0.26*	2.68 ± *0.04*

Table 4.3 Compressive properties of SAN model systems for the AN content effect study

	SAN19	**SAN27** (Hi MW)	**SAN27** (Lo MW)	**SAN35**
Modulus (GPa)	3.5 ± *0.1*	3.6 ± *0.1*	3.5 ± *0.2*	3.4 ± *0.2*
Yield Strength (MPa)	117.6 ± *0.8*	115.2 ± 0.5	117.2 ± 0.2	113.7 ± *1.4*
Yield Strain (%)	4.70 ± *0.59*	4.80 ± *0.25*	4.72 ± *0.27*	5.44 ± *0.08*
Secant Modulus at Yield Point (GPa)	2.50	2.40	2.48	2.09
Uni-axial Strain Hardening Exponent	1.35 ± *0.05*	1.33 ± *0.03*	1.37 ± *0.11*	1.43 ± *0.08*
Plane-Strain Hardening Exponent	1.68 ± *0.12*	1.70 ± *0.18*	1.71 ± *0.10*	1.55 ± *0.17*

4.3.2 Basic Scratch Mechanics

Before any fundamental scientific knowledge regarding the relationship between scratch deformation and mechanical properties can be gained, it is first necessary to understand the basic mechanics of the scratch process. In general, the scratch process involves a normal load applied to an asperity while in a sliding motion. This results in the application of multi-axial stress of compressive and tensile nature. However, the tip geometry and nature of the contact between the tip and its substrate can greatly affect the way the stress develops.

A schematic of contact between the spherical scratch tip and the deformed polymer substrate is given in Figure 4.3. The stress is highly localized where the center of the tip makes contact with the substrate. It then gradually diminishes away from the scratch tip. The applied stress under this contact scenario is, in reality, rather complex, but some assumptions can be made based on prior experiences with numerical modeling.

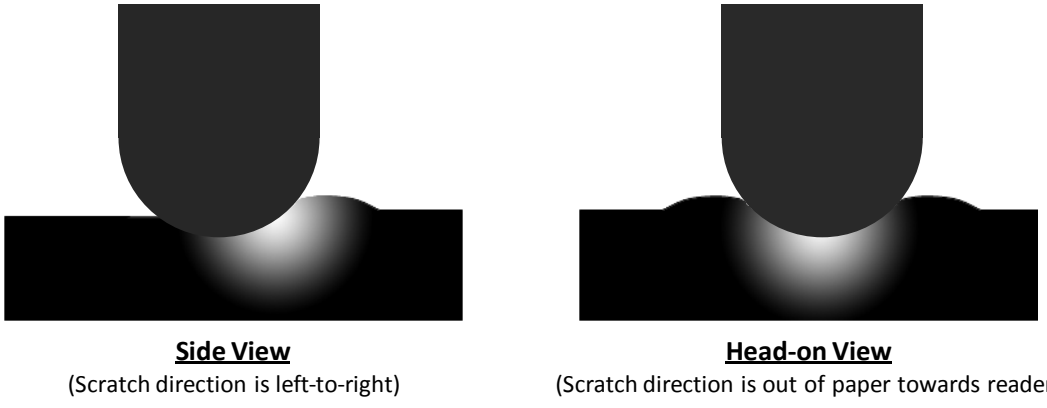

Figure 4.3 Schematic to illustrate contact geometry between scratch tip and polymer substrate.

The evolution of the von-Mises stresses during scratching with a spherical tip has been studied previously using FEM [66]. As shown from the schematic in Figure 4.4, the material will yield almost instantaneously upon contact, even under low loads, because the contact area of the tip is extremely small. Also, since the material in front of and underneath the tip is under compression, it is reasonable to assume that the nearly instantaneous yield is a dominated by compressive stress.

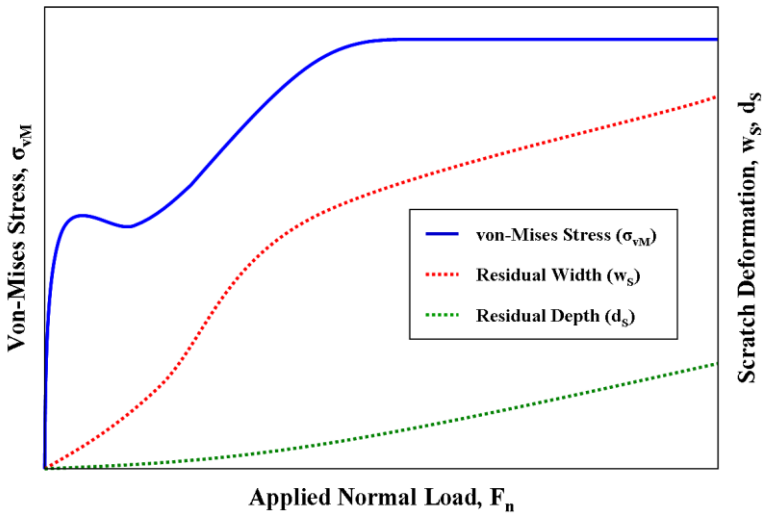

Figure 4.4 Development of von-Mises and scratch deformation as a function of applied normal load.

As the load progresses, tensile stress begins to develop as a result of increasing frictional force. The modeling effort discussed earlier also analyzed the tensile stress in the material with FEM [66]. An illustration of how these tensile stresses develop with respect to the applied normal load is given in Figure 4.5. According to the modeling results, the tensile stress develops behind the tip first. The direction of the maximum

principal tensile stress behind the tip is in the direction of the movement of the scratch tip and can largely be regarded as uni-axial tension dominant.

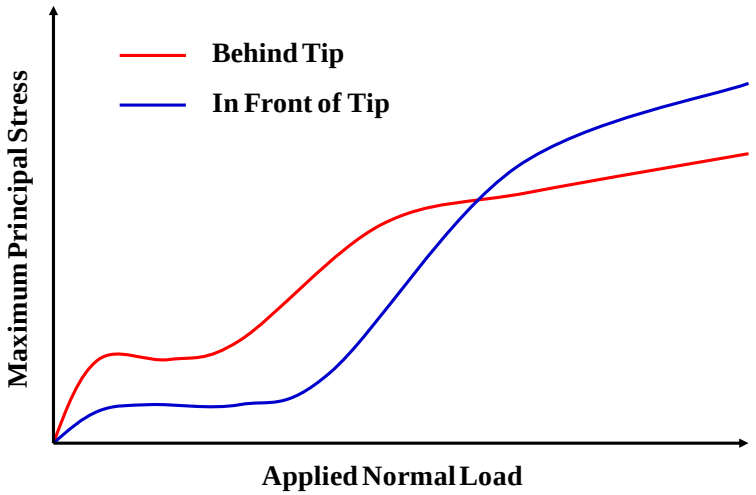

Figure 4.5 Development of tensile stresses around the scratch tip as a function of applied normal load.

As the load increases even further, the maximum tensile stress develops in front of the tip as the tip penetrates deeper and material continues to deform. The direction of the maximum principal stress in front of the tip is in a direction perpendicular to the scratch tip movement. The tensile stress in front of the tip causes removal of material from the scratch path. It should be noted that the tensile stress behind the tip is still present.

With this understanding of the basic mechanics of the progressive load scratch process, it is now possible to make inferences as to how each deformation mechanism is related to the mechanical properties of the polymer. To begin, a parametric study using

numerical simulation was carried out to investigate the effects of key material parameters like Young's modulus, Poisson's ratio, yield strength and coefficient of friction on polymer scratch behavior [63]. To simplify the study, a linearly elastic/perfectly plastic material was modeled. By using this model, there were no complications from post-yield behavior; the material simply fails after surpassing its elastic limit. The study concluded that, regarding scratch performance, yield strength and coefficient of friction had the most impact in improving scratch performance. These analyses provided the basis for important fundamental insights regarding the fundamental understanding of polymer scratch behavior.

4.3.3 Scratch Damage Mechanisms & Correlation with Mechanical Properties

Images of the SAN model systems scratched at 1, 10 and 100 mm/s as obtained with the PC scanner are shown in Figure 4.6. The usefulness of the ASTM progressive load methodology is displayed here in that the gradual evolution of the applied stress allows for the observation of several transitions in the scratch damage mechanisms. The apparent rate-sensitivity for these damage mechanisms will be addressed in the following sections.

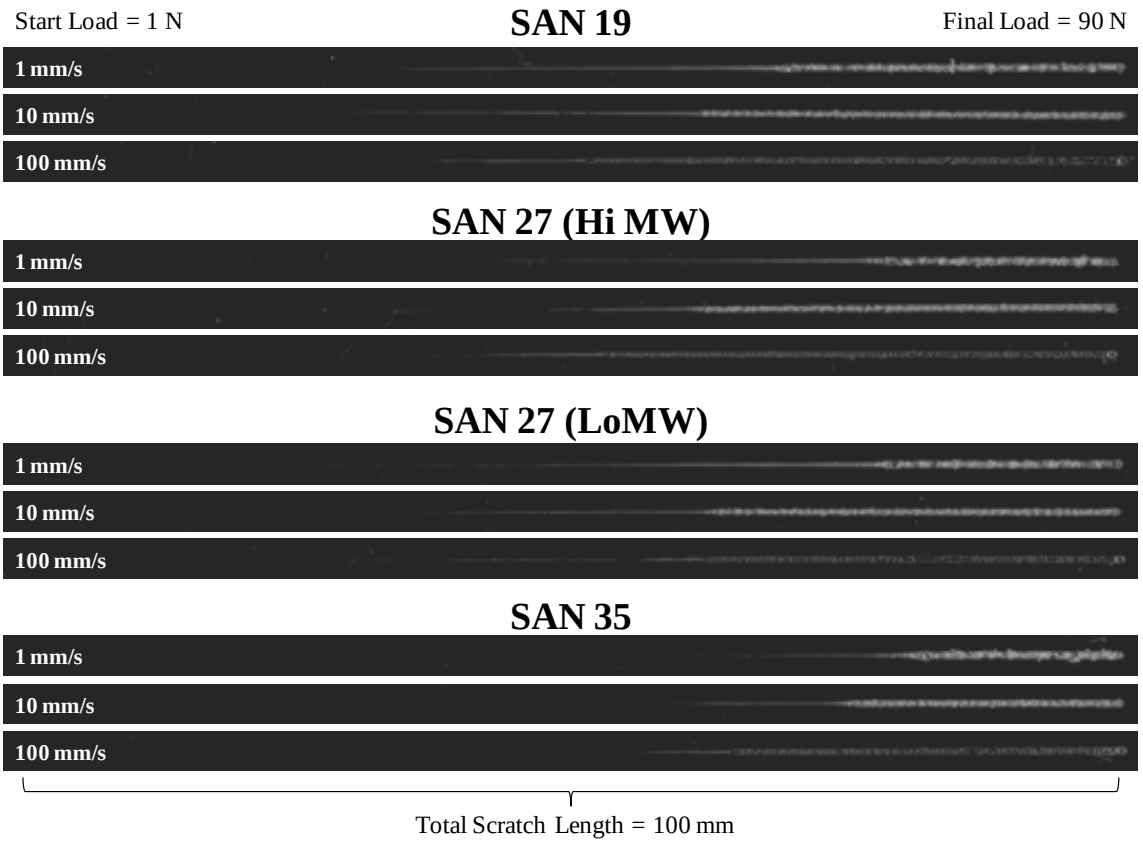

Figure 4.6 Optically scanned images of scratched SAN model systems with varying AN content. (Resolution = 300 dpi)

Upon microscopic examination of the scratched samples, four main scratch damage mechanisms have been identified for SAN and are listed in the order that they occur as the applied normal load progressively increases:

- Scratch groove formation – First depth deviation from the flat, virgin surface condition within the scratch path.
- Scratch visibility – The intensity of scattered incident light has reached a point to introduce sufficient contrast relative to the virgin background to become visible to human eyes.

- Periodic micro-cracking – Brittle surface failure induced by the scratch tip causes cracking that is periodic in nature due to the stick-slip phenomenon [65].
- Plowing –The scratch tip has penetrated through the surface of the polymer, resulting in failure where material is fractured and removed as chip-like debris or a machined ribbon, depending on the test speed.

A schematic illustrating the groove formation, cracking and plowing mechanisms is given in Figure 4.7.

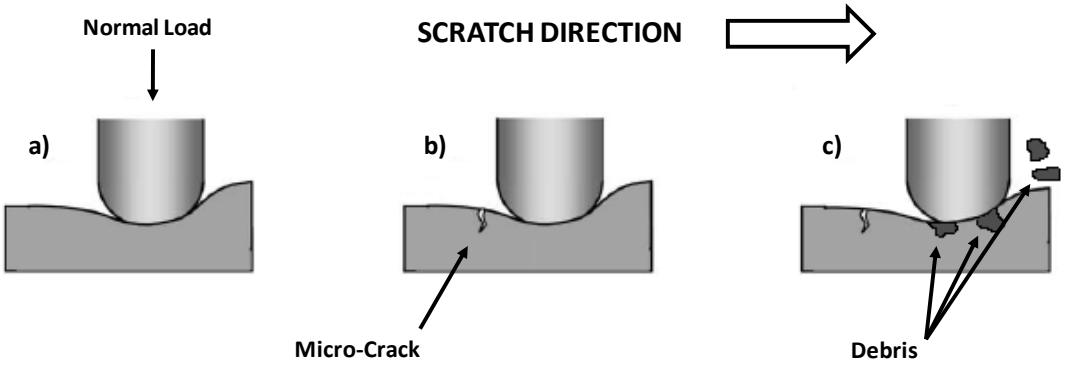

Figure 4.7 Schematic of scratch damage mechanisms: a) Groove formation; b) Periodic micro-cracking; c) Plowing.

The groove formation, micro-cracking and plowing mechanisms are related to the mechanical properties of the SAN model systems and corresponding correlations will be established below.

4.3.3.1 Scratch Groove Formation

In the beginning of the scratch, the applied stress is low and any scratch deformation will be largely recoverable. However, soon after the beginning of the

scratch, non-recoverable plastic deformation will take place in the formation of a scratch groove. From a topographical point of view, the formation of a scratch groove happens at the first point where the scratch depth has deviated from the undamaged, virgin surface after the material has viscoelastically recovered for at least one day.

A 3-D profile of a typical scratched SAN sample as measured with the VLSCM can be seen in Figure 4.8. The groove formation can be clearly seen here. Furthermore, the first sign of scratch groove formation can be observed when the height profile of the scratch is compared to that of the surrounding virgin surface as shown in Figure 4.9.

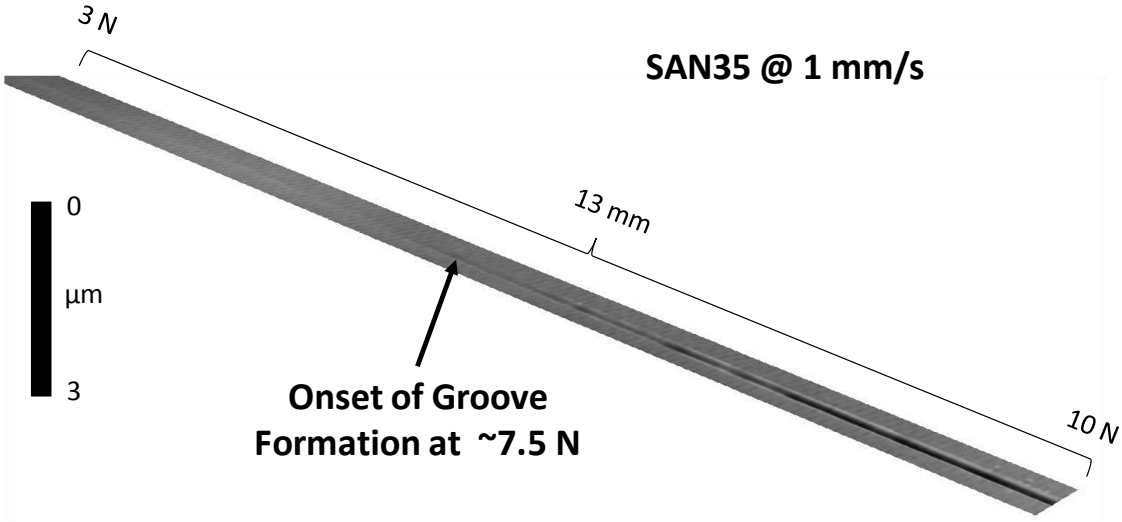

Figure 4.8 3-D profile (*via* VLSCM) of a typical scratched sample of SAN showing the onset of scratch groove formation.

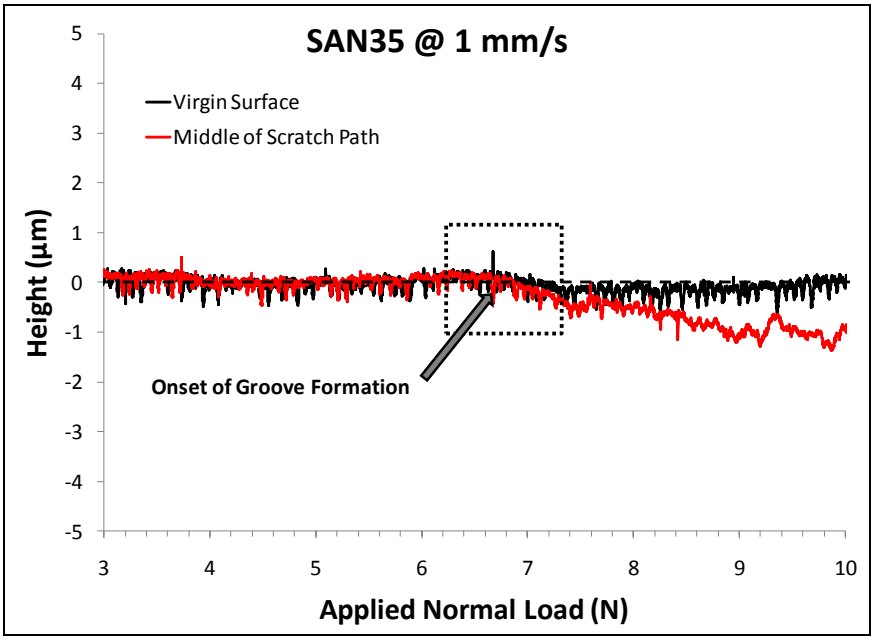

Figure 4.9 Height profiles (*via* VLSCM) of a scratch in a typical SAN model system and its corresponding virgin surface.

As mentioned in Section 2, the applied stress at the onset of groove formation is compression-dominant. It is perhaps intuitive to assume that the compressive yield stress alone can be used to assess how resistant the material is to scratch groove formation. However, since the stresses exerted on the polymer substrate depend on the amount of surface contact between the scratcher tip and the substrate, the conformability of the substrate to the scratcher tip geometry before yielding should also be considered. As a result, a better metric to account for both of the factors mentioned above is the secant modulus at the yield point (i.e. the ratio of stress and strain at the compressive yield point).

The values for secant modulus at compressive yield and critical load for onset of groove formation are shown as a function of AN content in Figures 4.10 and 4.11,

respectively. The overall trend in the results points to the fact that increasing the AN content lowers the secant modulus. At the same level of MW, increasing the AN content appears to delay the onset of groove formation with the most effect seen at higher MW.

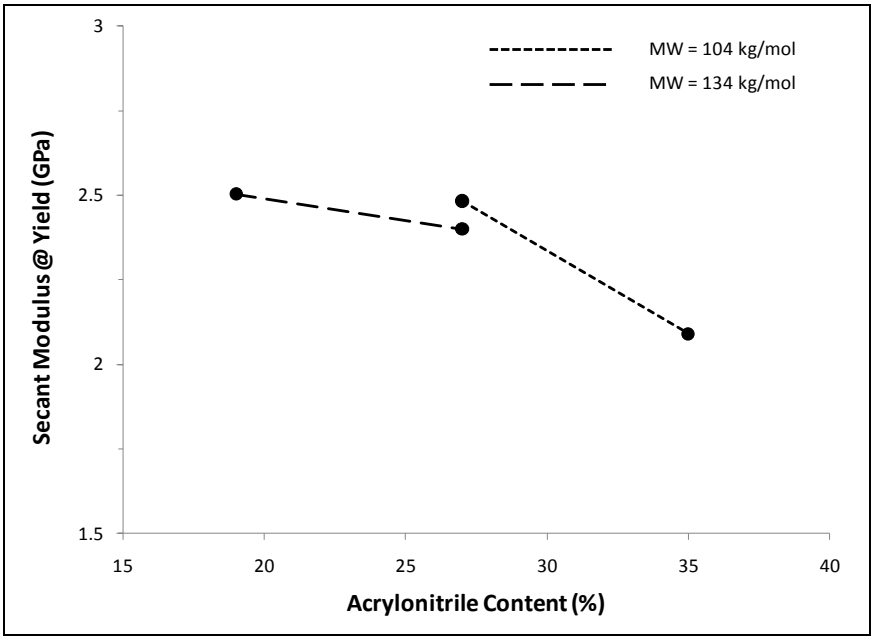

Figure 4.10 Secant modulus at compressive yield point for SAN model systems as a function of AN content.

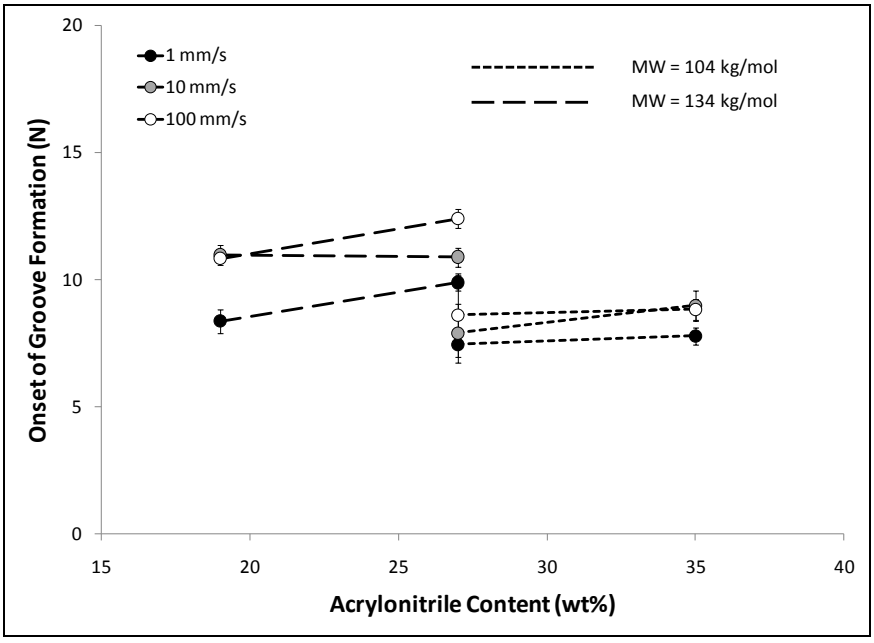

Figure 4.11 Critical load for the onset of groove formation for SAN model systems as a function of AN content.

Figure 4.12 shows the correlation of secant modulus at compressive yield point with the critical load for the onset of scratch groove formation. The fact that a higher secant modulus is related to earlier groove formation may simply be due to a less amount of surface contact between the scratcher tip and the substrate is reached at the same applied normal load, leading to a higher stress magnitude experienced by the substrate. On the other hand, in a material with a lower secant modulus subjected to the same applied load, the deformation and contact area will be large and the applied stress small. The onset of groove formation will be delayed as a result. In short, the secant modulus at the compressive yield point shows a mechanically sound correlation with the onset of scratch groove formation. It should be noted however, that this correlation only stands when the difference in the yield strength of the systems is small.

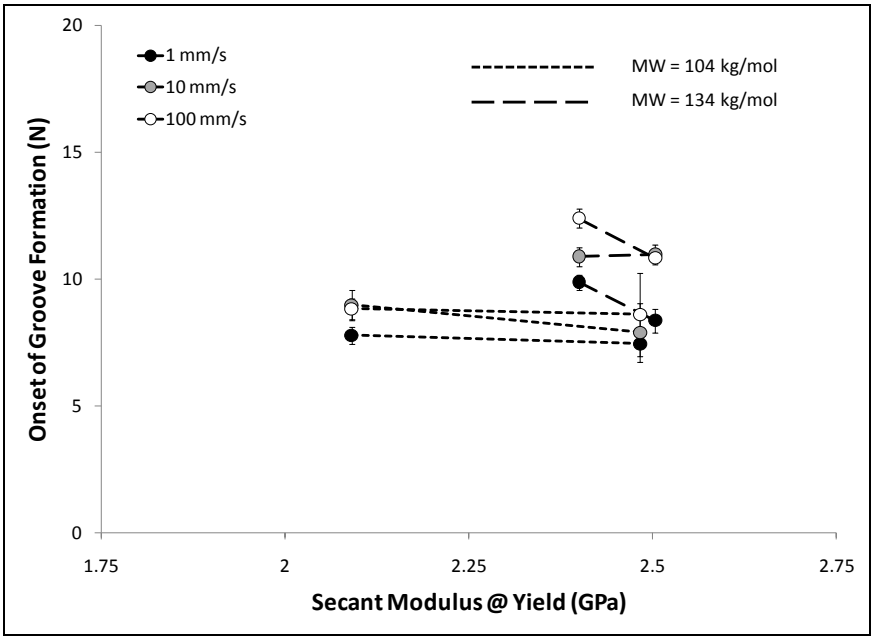

Figure 4.12 Critical load for the onset of groove formation as a function of secant modulus at the compressive yield point for SAN model systems with varying AN content.

4.3.3.2 Periodic Micro-Cracking

As mentioned before, tensile stress behind the tip develops as the applied normal load increases. As the uni-axial tensile curves in Figure 4.1 show, the SAN model systems of this study show no signs of post-yield behavior under tension. That means that when the ultimate tensile strength in the material is reached, the material will fail in a brittle fashion. Likewise, when the tensile stress behind the scratch tip develops to the level of the ultimate tensile strength, failure should occur in the form of a crack. After the onset of cracking, the deformation will continue as a series of periodic cracks as a result of the well-known stick-slip phenomenon [65]. The high-resolution VLSCM micrograph shown in Figure 4.13 is representative of this damage feature at its onset.

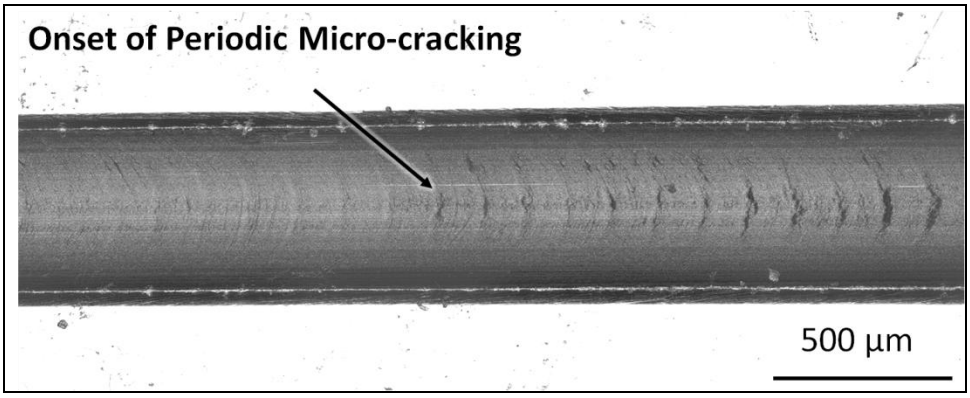

Figure 4.13 Optical image from a laser confocal microscope (VLSCM) of typical periodic micro-cracking scratch damage observed in SAN model systems.

The tensile strength and the onset of periodic cracking for the model systems are shown as a function of AN content in Figures 4.14 and 4.15, respectively. Here, the AN content appears to have a noticeable effect on the tensile behavior. A higher AN content also seems to delay the onset of periodic cracking. As discussed earlier, the tensile stress behind the scratch tip can be regarded as uni-axial tension dominant. Therefore, the onset of periodic cracking should be largely related to the uni-axial tensile strength. Figure 4.16 shows the onset of periodic cracking as a function of tensile strength at each testing speed. The resulting general trend is intuitive; a higher tensile strength will result in a delayed onset of periodic cracking with little effect seen from MW. As the tensile strength is positively related to the AN content, these results point to the fact that a higher level of AN content will result in better scratch resistance by delaying the onset of periodic cracking. Scratch speed appears to have some influence on the onset of periodic micro-cracking and seems more apparent at higher levels of AN content.

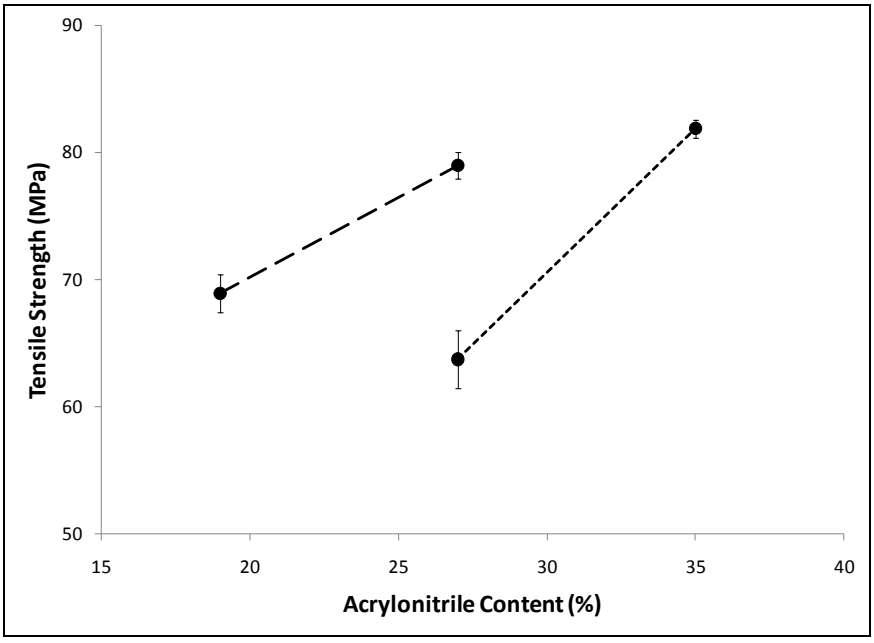

Figure 4.14 Tensile strength of SAN model systems as a function of AN content.

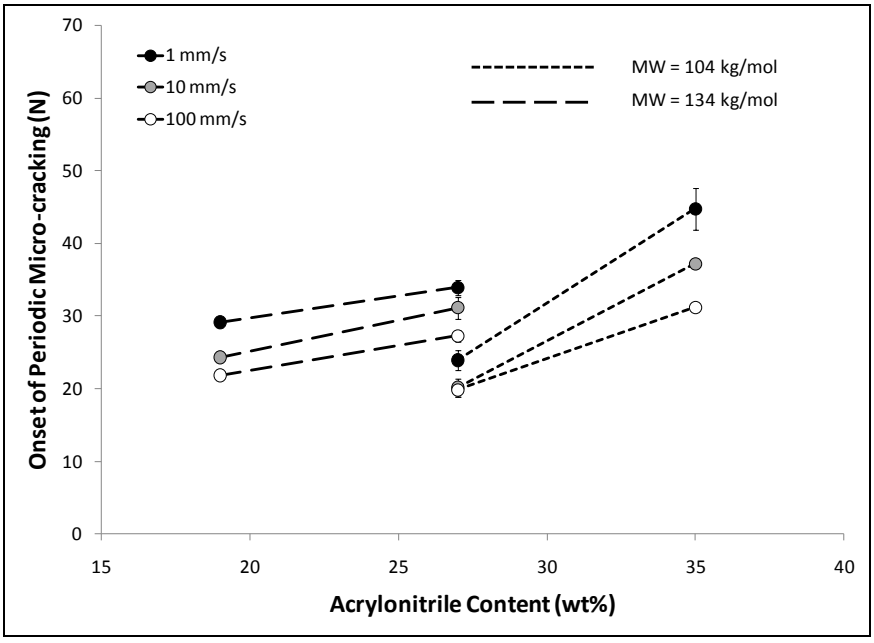

Figure 4.15 Critical load for the onset of periodic micro-cracking as a function of AN content for SAN model systems.

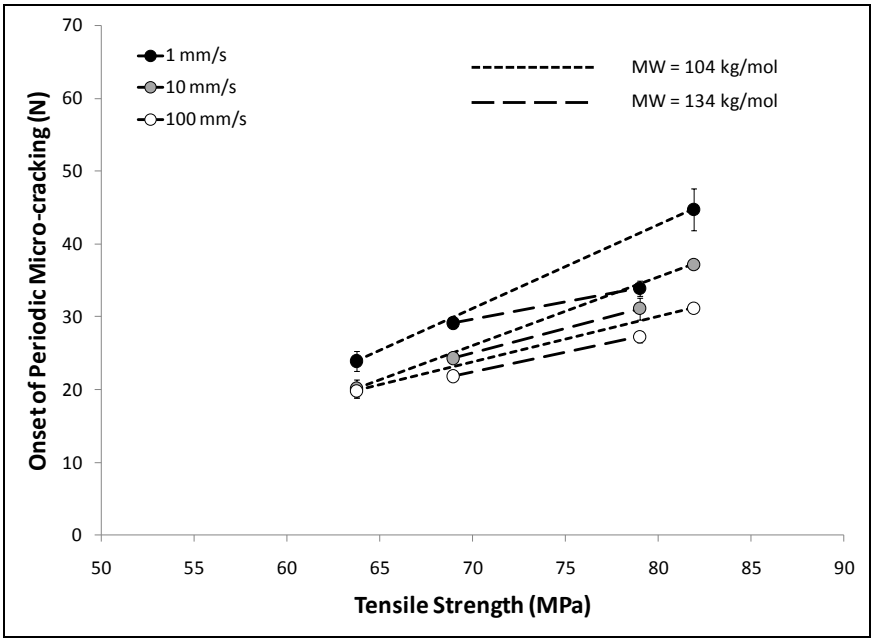

Figure 4.16 Critical load for the onset of periodic micro-cracking as a function of tensile strength for SAN model systems with varying AN content.

4.3.3.3 Plowing

As mentioned, the tensile stress in front of the tip will eventually develop to dominate the scratch deformation. This is a result of the material in front of the tip being shored-up and forced to the side, forming what is sometimes referred to as "pile-up" [65]. The direction of this tensile stress is perpendicular to the stress ahead of the tip. Eventually, the total stress applied to the system will surpass the ultimate strength of the material and penetrate through its top surface. Once this occurs, the tip will begin to remove and displace material in front of and around it in a plowing fashion. At this point, the material is actually fractured completely and is removed in the form of a machined ribbon or debris, depending on the testing speed. A VLSCM micrograph representative of this damage feature is shown in Figure 4.17.

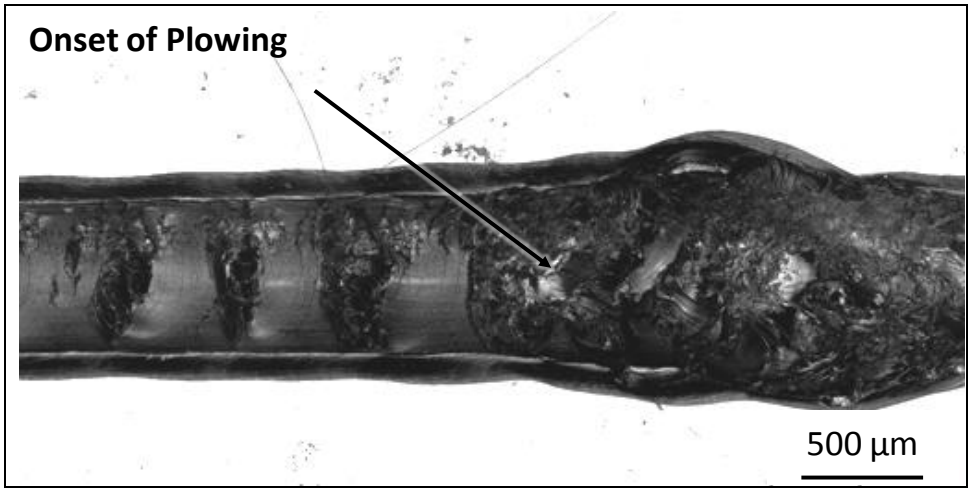

Figure 4.17 Optical image from a laser confocal microscope (VLSCM) of typical plowing scratch damage observed in SAN model systems.

Figure 4.18 shows that increasing the AN content definitely results in a delayed onset of the plowing mechanism. Since it was shown that this mechanism is caused by tensile failure, the onset of plowing is correlated with tensile strength in Figure 4.19. As with the micro-cracking mechanism, a higher AN content leads to a higher tensile strength and will give a delayed onset of plowing. Scratch speed apparently strongly influences the onset of the plowing mechanism while MW does not show a strong effect. Speculations as to why will be made in a later section.

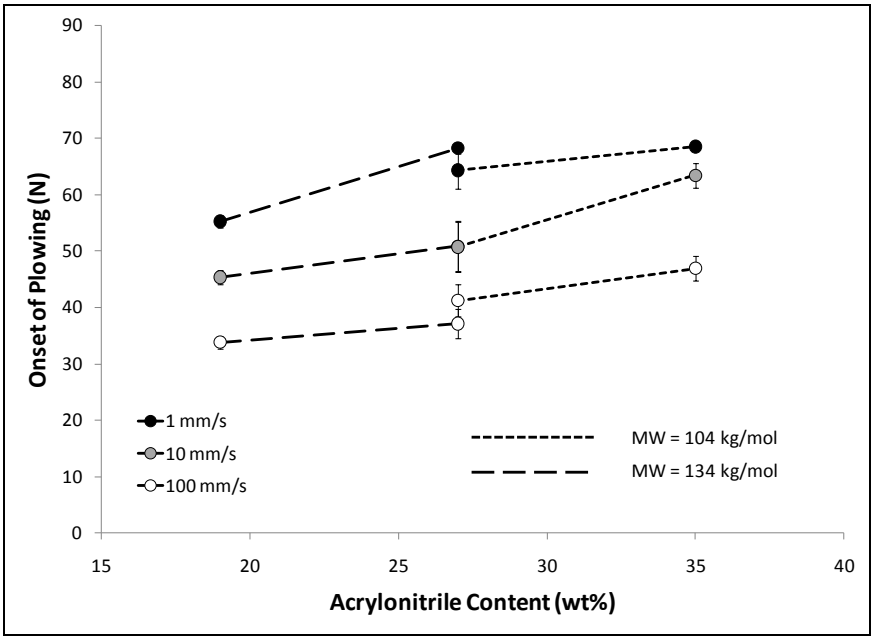

Figure 4.18 Critical load for the onset of plowing for SAN model systems as a function of AN content.

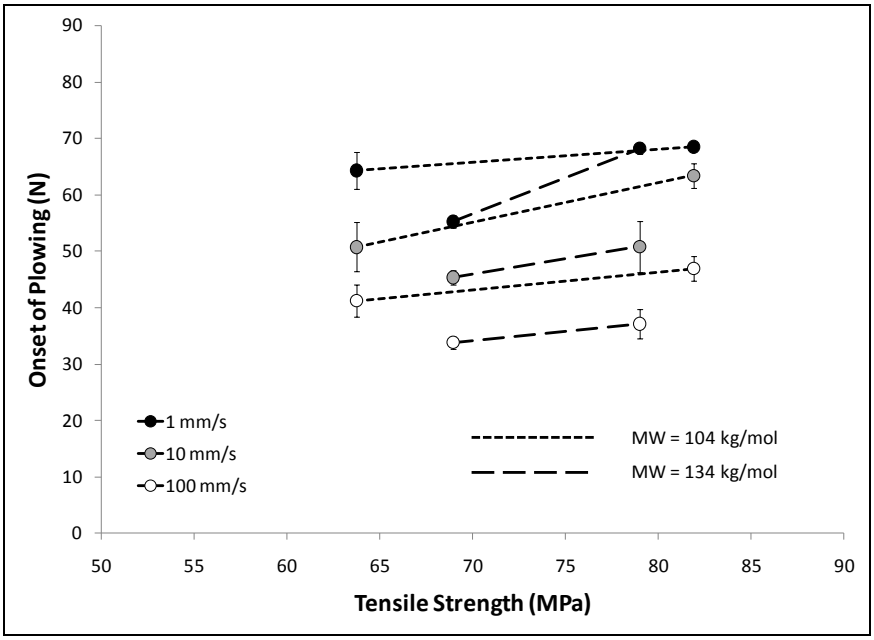

Figure 4.19 Critical load for the onset of plowing as a function of tensile strength for SAN model systems with varying AN content.

4.3.4 Scratch Visibility

In the previous section, it was stated that a scratch can be considered visible to average human eyes when the contrast between the scratch damage and the virgin background reaches a level of 2% for high gloss surfaces. This criterion, along with the fact that the smallest feature size a human eye can resolve is 90 μm, was used to evaluate the scratch visibility resistance of the SAN model systems with the ASV® software. The 90% continuity criterion was employed, as well.

The previous section also showed that the orientation from which a scratch is illuminated could influence the assessment of scratch visibility. When the light source is oriented parallel to the scratch path, the roughness of the surface of the scratch path will be the main cause of scratch visibility. In a perpendicular orientation, the scratch will become visible when the shoulder on the sides of the scratch reaches a critical height (i.e. visibility in the perpendicular illumination orientation occurs as a result of plastic deformation). This same protocol was employed to assess the scratch visibility of the SAN model systems in this study.

The critical load for the onset of scratch visibility (*via* ASV®) at each testing speed and for each orientation is given as a function of AN content in Figures 4.20 and 4.21. From these results, it can be said that SAN35 is the only model system significantly affected by illumination orientation effects. To illustrate the orientation effect, processed images of SAN35 at each testing speed are shown in Figure 4.22.

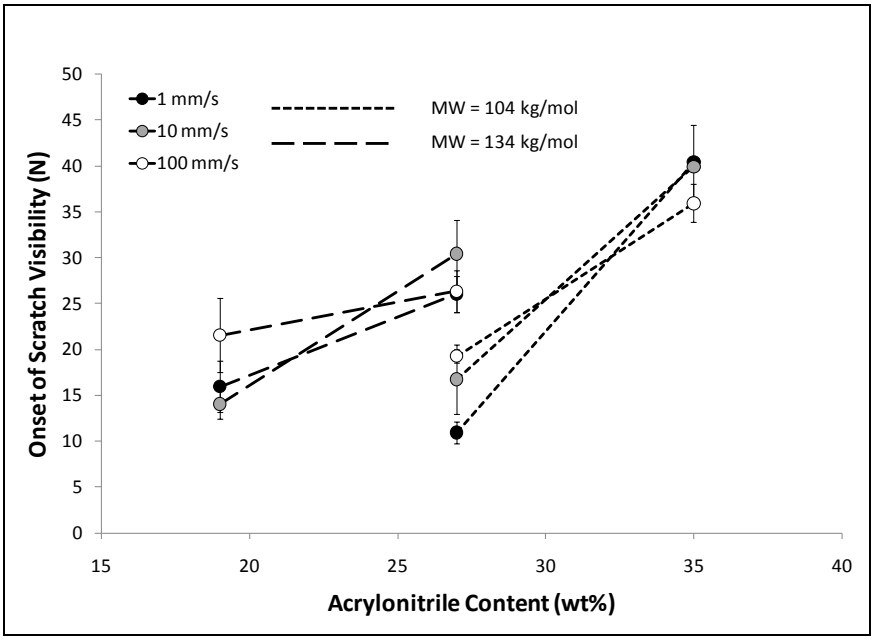

Figure 4.20 Critical load for the onset of visibility for parallel illumination orientation.

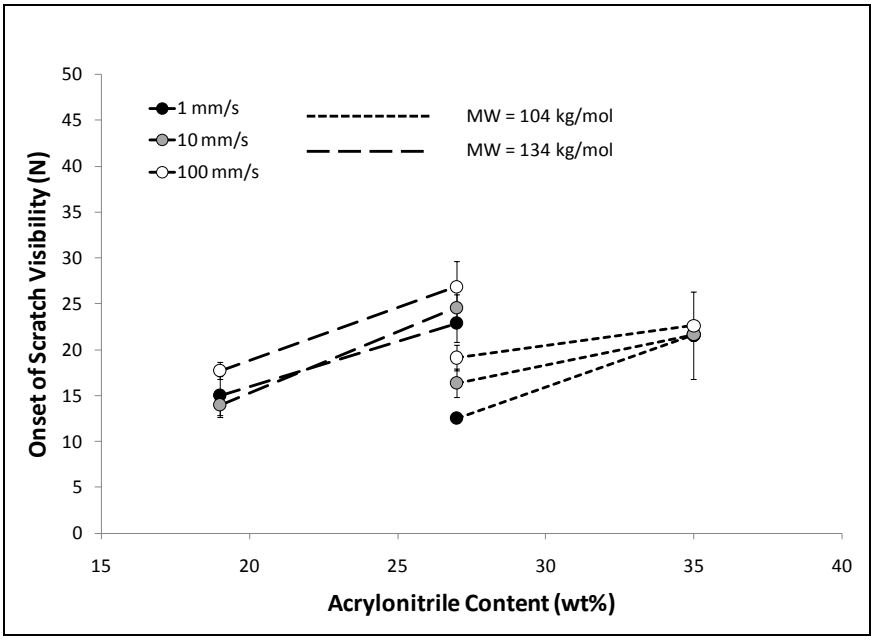

Figure 4.21 Critical load for the onset of visibility for perpendicular illumination orientation.

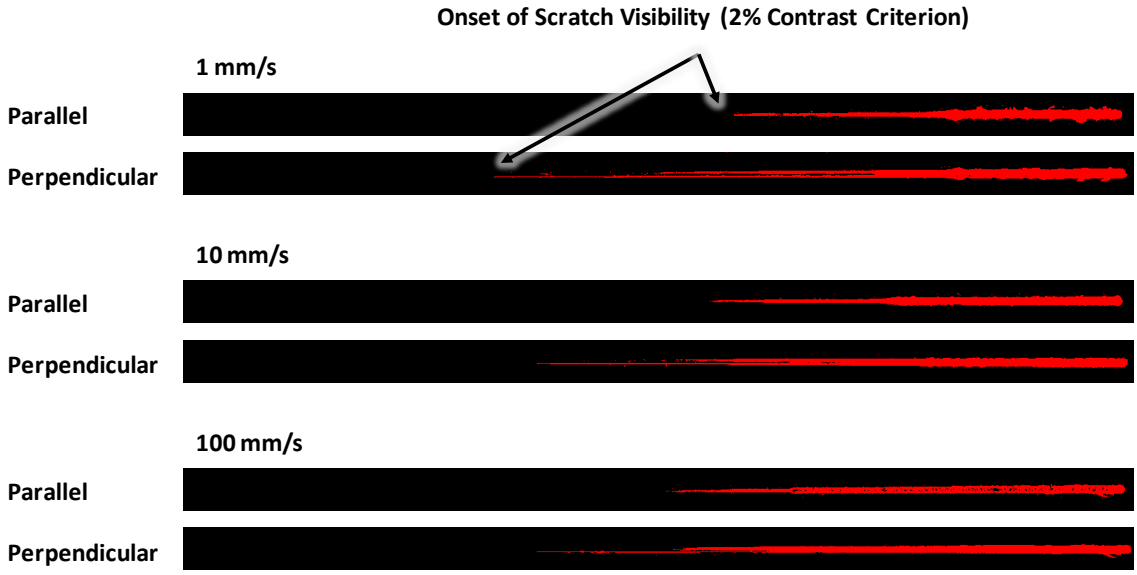

Figure 4.22 Images of SAN 35 processed by ASV® software.

Since the origins and physics of scratch visibility were outlined in the PVC/PP study of the previous section, the same analysis was carried out on the SAN model systems. Since the methodology is simply being repeated and applied to the SAN systems, the results will not be shown here. For the SAN model systems of this study, the RMS roughness of the scratch path to induce visibility in parallel orientation is ~300 nm. For perpendicular orientation, the shoulder height was on the order of 2 – 4 μm in order for the scratch to be visible.

The AN content can change the location at which the roughness or shoulder height reaches its critical level. As shown in Figures 4.20 and 4.21, there appears to be a positive trend where increasing the AN content will delay the onset of scratch visibility. With regards to scratch path roughness (i.e. parallel orientation), SAN35 shows the highest level of scratch visibility resistance. The same trend can be seen in plastic

deformation (i.e. perpendicular orientation), but the dominance of SAN35 is more marginal. This could suggest that a higher AN content will not likely effect the resistance to plastic scratch deformation, but could possibly impart resistance to surface roughening. The scratch speed does not seem to strongly affect the onset of scratch visibility under the conditions of this study while increasing the molecular weight tends to improve scratch visibility resistance. The molecular weight effect will be addressed in more detail in the next section.

4.3.5 Frictional Behavior

The scratching coefficient of friction (SCOF) is defined as the ratio of the tangential force and the applied normal load throughout the scratch. The SCOF for the SAN model systems at each test speed is shown in Figures 4.23 – 4.25 as a function of scratch length. The large magnitude of fluctuation at the beginning of the test is due to inertial effects from instantaneously accelerating the scratch head to the designated scratch speed.

Figure 4.23 shows that SAN 35 has the lowest SCOF of the three model systems. At 100 mm/s (Figure 4.25), the difference is not as noticeable. This could be attributed to the fact that at the highest scratch speed, the SAN systems all respond in a similar brittle fashion. It was stated earlier that the micro-cutting mechanism exhibits the highest dependence on scratch speed. The SCOF in the last portion of the scratch is related to the plowing mechanism.

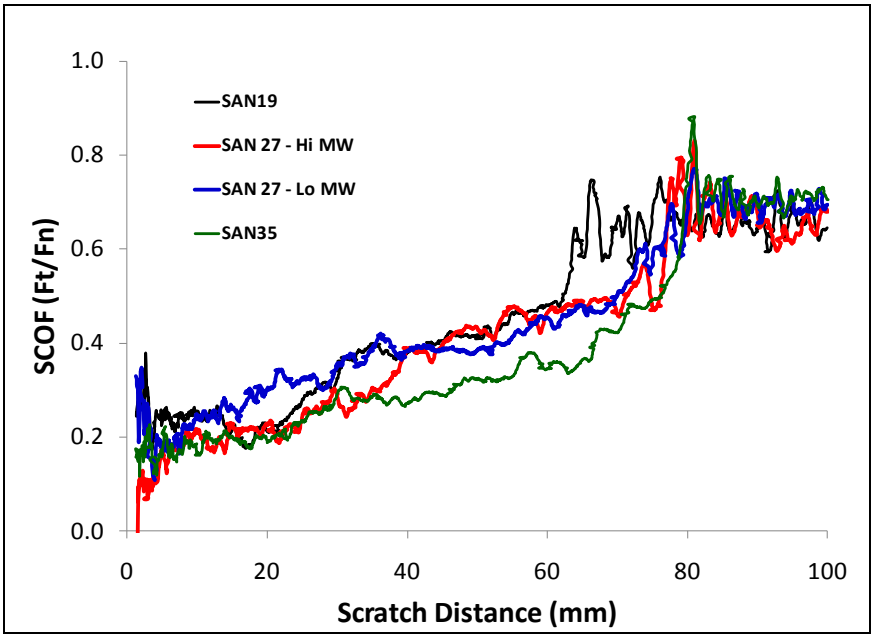

Figure 4.23 Scratch coefficient of friction as a function of scratch distance for SAN model systems with varying AN content. (Scratch speed = 1 mm/s)

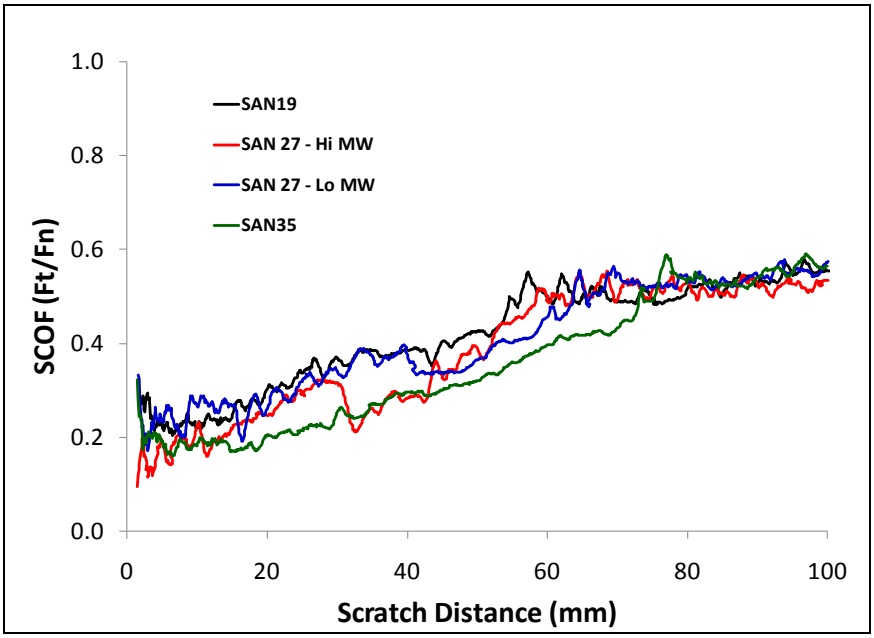

Figure 4.24 Scratch coefficient of friction as a function of scratch distance for SAN model systems with varying AN content. (Scratch speed = 10 mm/s)

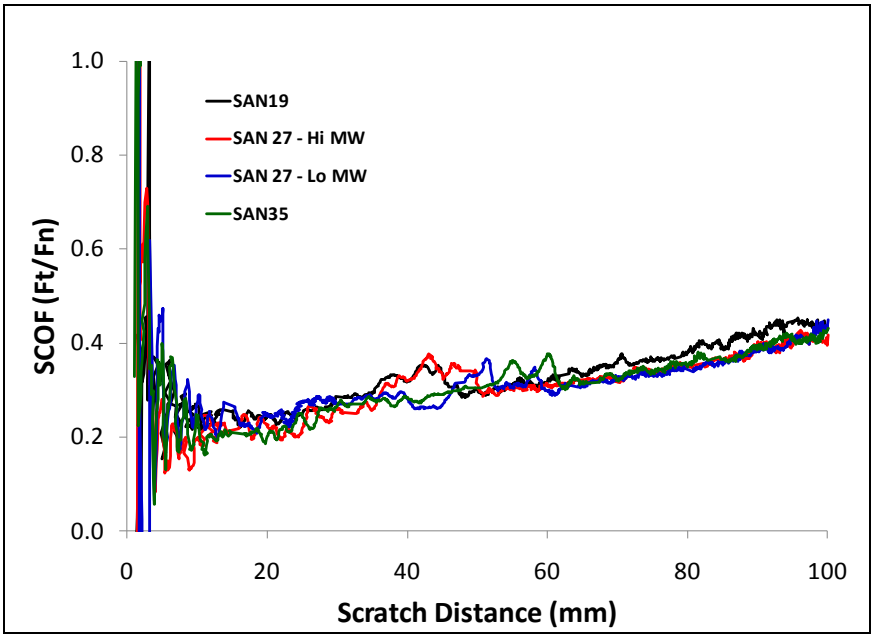

Figure 4.25 Scratch coefficient of friction as a function of scratch distance for SAN model systems with varying AN content. (Scratch speed = 100 mm/s)

The SCOF curves suggest three main points:

1. The SCOF related to the plowing mechanism is not dependent on AN content or MW.
2. The SCOF related to plowing will be quite high at slow scratch speeds and will decrease with increasing scratch speed.
3. At slow speeds, the material in front of the tip imparts a significant amount of resistive (i.e. tangential) force, thus resulting in a high SCOF. However, as the speed increases, the response of the polymer becomes more rigid and brittle and the ability of the material to withstand the applied stress decreases. Therefore, the resistive force, as well as the SCOF, will be lower.

In the numerical parametric study mentioned earlier, it was found that decreasing the coefficient of friction of a polymeric material resulted in enhanced scratch resistance [63]. Of the model systems studied in this section, SAN35 definitely shows the best scratch resistance in general, but the parametric study also showed that increasing the tensile strength of the material gave better scratch resistance, as well. Therefore, it is difficult to ascertain if the SCOF, the tensile properties or the combination of both is responsible for the superior scratch resistance of SAN35.

5. EFFECT OF MOLECULAR WEIGHT ON SCRATCH BEHAVIOR OF SAN MODEL SYSTEMS

Molecular weight (MW), which is directly related to chain length, thus entanglement density, is one of the most important material attributes that contributes to mechanical integrity of thermoplastics [1]. When MW is small, the molecular chains do not have sufficient entanglement to exert mechanical integrity. As a result, the polymer is rather weak. On the other hand, as the MW increases past its characteristic entanglement MW, M_e, the tensile strength of the polymer will increase significantly [89]. Since the model systems of Section 4 had variations of both AN content and MW, it was difficult to ascertain how much influence MW has on the scratch behavior of SAN. This section focuses on probing how the MW can influence on the scratch behavior of SAN random copolymers. The same analyses of scratch deformation mechanisms are used as in Section 4 and general implications of material properties on polymer scratch behavior are discussed.

5.1 Model SAN Systems

The SAN model systems for this part of the study contain 27 wt% AN and were provided by BASF SE with varying levels of molecular weight. The resins were prepared and injection-molded in an identical manner as the model systems in Section 4. Upon receipt, the same annealing and post-annealing analysis was carried out. Physical properties and MW of the SAN systems investigated here are given in Table 5.1.

Table 5.1 Physical properties of SAN model systems for the molecular weight effect study

	SAN 27 A	SAN 27 B	SAN 27 C
Acrylontrile Content (wt%)	27	27	27
Molecular Weight (kg/mol)	106	119	134
Polydispersity	4.4	4.3	3.9
Poisson's Ratio	0.35	0.35	0.35

5.2 Experimental Procedures

All procedures regarding tensile and compression testing, ASTM/ISO scratch testing and microscopic analyses were the same as described as in Section 4.

5.3 Results and Discussion

5.3.1 Mechanical Properties of Model Systems

The stress-strain curves for the model SAN systems under uni-axial tension are shown in Figure 5.1. Under compression, the only appreciable difference observed between the uni-axial and plane-strain compression stress-strain curves was the strain-hardening exponent. Therefore, only a typical compressive stress-strain curve for the SAN systems is shown in Figure 5.2. The tensile and compressive properties are summarized in Tables 5.2 and 5.3.

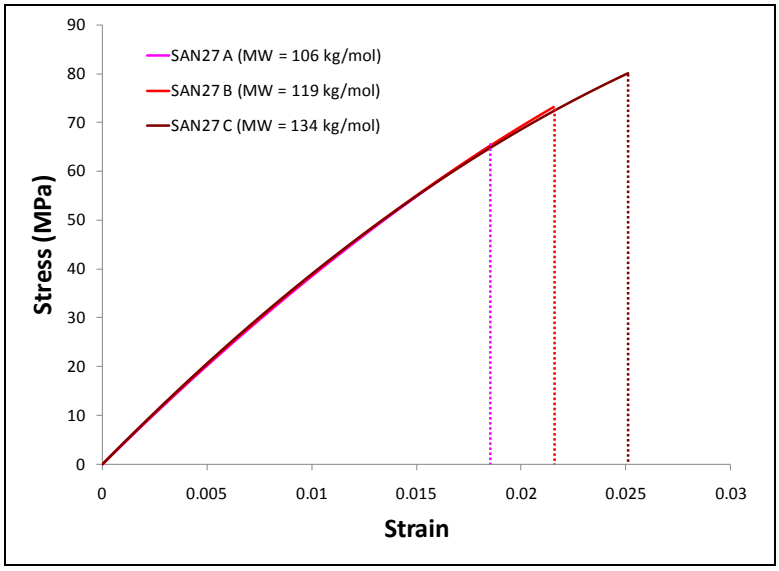

Figure 5.1 Stress-strain curves of model SAN systems with varying molecular weight under uni-axial tension.
(**NOTE** - The vertical lines are meant to differentiate the strain at break for the systems and are not a representation of unloading behavior.)

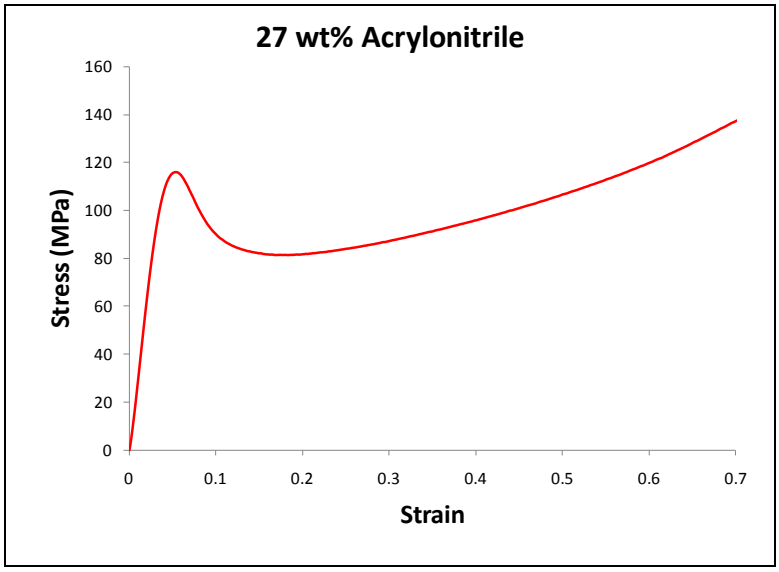

Figure 5.2 Typical compressive stress-strain curve for SAN model systems with varying molecular weight.

Table 5.2 Uni-axial tensile properties of SAN model systems for the molecular weight effect study

	SAN27 A	**SAN27 B**	**SAN27 C**
Modulus (GPa)	3.6 ± *0.1*	3.7 ± *0.1*	3.7 ± *0.1*
Tensile Strength (MPa)	63.7 ± *2.3*	75.1 ± *3.0*	79.0 ± *1.0*
Ductility (%)	1.9 ± *0.2*	2.4 ± *0.1*	2.6 ± *0.1*

Table 5.3 Compressive properties of SAN model systems for the molecular weight effect study

	SAN27 A	**SAN27 B**	**SAN27 C**
Modulus (GPa)	3.5 ± *0.2*	3.6 ± *0.3*	3.6 ± *0.1*
Yield Strength (MPa)	117.2 ± 0.2	117.2 ± 0.4	115.2 ± 0.5
Yield Strain (%)	4.7 ± *0.3*	4.8 ± *0.5*	4.8 ± *0.2*
Secant Modulus at Yield Point (GPa)	2.48	2.44	2.40
Uni-axial Strain Hardening Exponent	1.33 ± *0.05*	1.38 ± *0.10*	1.33 ± *0.03*
Plane-Strain Hardening Exponent	1.71 ± *0.10*	1.61 ± *0.02*	1.70 ± *0.18*

5.3.2 Scratch Behavior and Correlations with Mechanical Properties

As an example of the overall appearance of the scratch deformation, scanned images of the SAN model systems scratch tested at 1 mm/s are given in Figure 5.3. The corresponding images after processing with ASV© are also shown in Figure 5.3. The Roman numerals in Figure 5.3 correspond to the four key scratch damage transitions for SAN that were identified and described in Section 4.

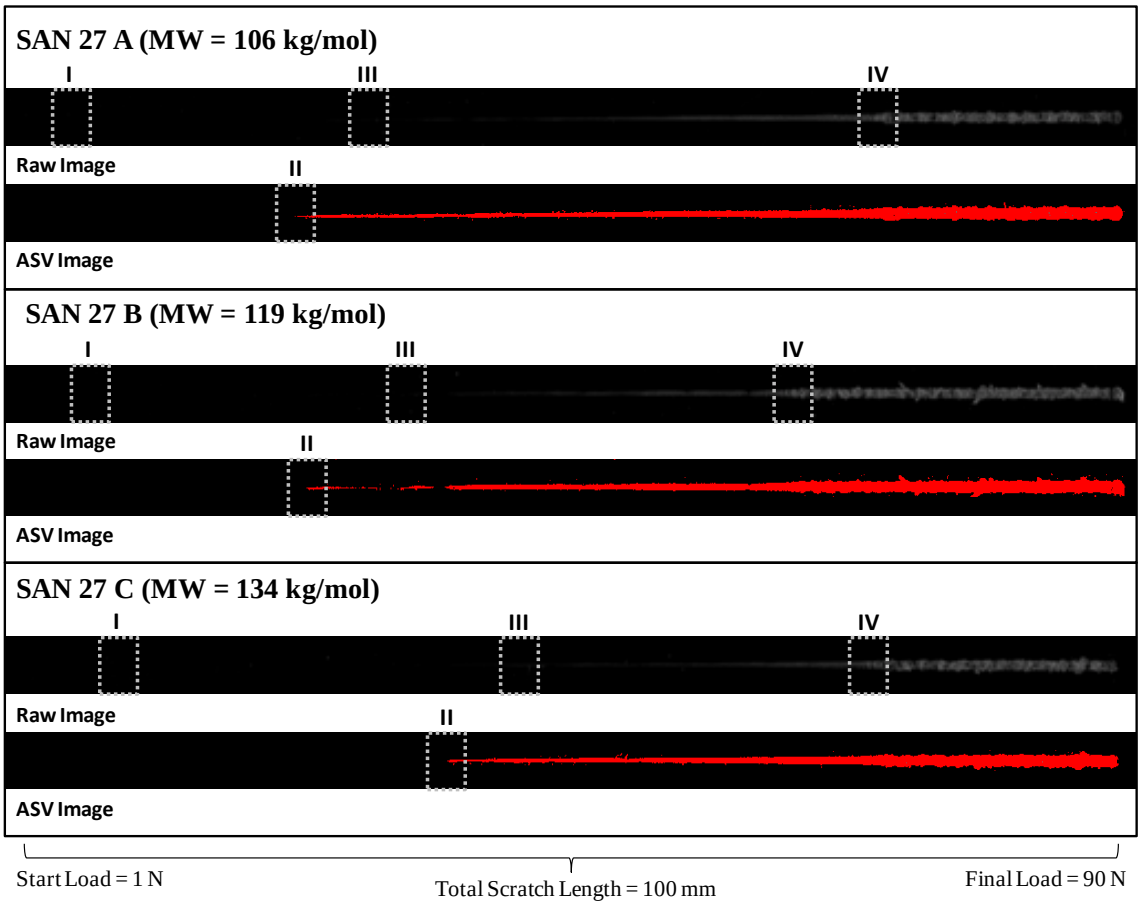

Figure 5.3 Digital images of scratch tested SAN model systems after scanning at 300 dpi and accompanying images after processing with ASV® software.

In the previous study, it was found that the secant modulus at compressive yield and the tensile strength were good metrics for establishing correlations between mechanical properties and scratch deformation. The compressive yield secant modulus will give a measure of the conformability of the polymer substrate to the indenter prior to yielding. When this modulus is relatively low, the material will experience a larger contact area under compression (i.e., lower stress) and will likely delay scratch groove formation. Periodic micro-cracking and plowing occur as a result of the formation of

tensile stresses behind and in front of the scratch tip, respectively. In that respect, the compressive yield secant modulus and tensile strength are shown as a function of MW in Figures 5.4 and 5.5, respectively. It can be seen that increasing the MW results in a decrease of the secant modulus and an increase in the tensile strength.

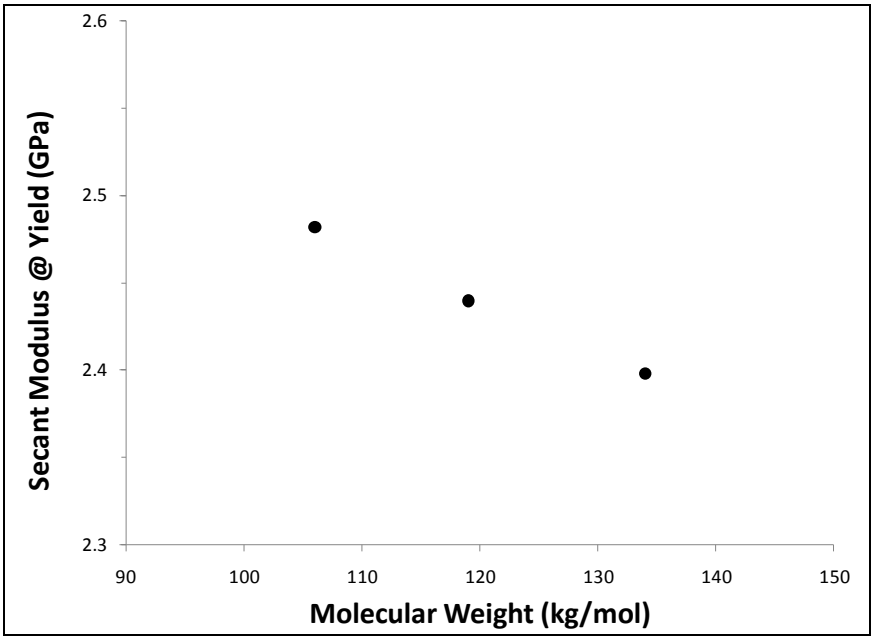

Figure 5.4 Secant modulus at compressive yield point for SAN model systems as a function of molecular weight.

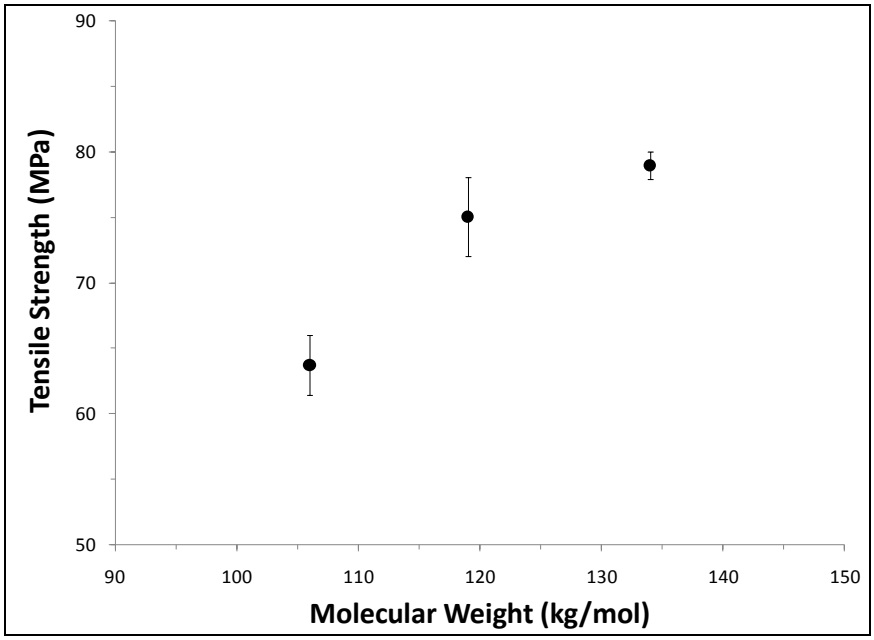

Figure 5.5 Tensile strength of SAN model systems as a function of molecular weight.

5.3.2.1 Scratch Groove Formation

Scratch groove formation is a result of non-recoverable deformation and was defined in Section 4 as the point where the height profile of the scratch path begins to continuously deviate from that of the virgin surface. Figs. 5.6 and 5.7 show the onset of groove formation as a function of MW and compressive yield secant modulus, respectively. Increasing the MW will slightly delay the onset of groove formation Furthermore, since increasing the MW was shown to decrease the compressive yield secant modulus, it is now clear that a lower secant modulus is related to resistance against scratch groove formation. This finding is consistent with what was found in the previous study regarding the AN content effect. Again, this correlation is only true when the difference in the yield strength of the systems is small. In short, decreasing the

compressive yield secant modulus of a polymeric material is likely a favorable way to impart resistance against the formation of the first signs of scratch deformation.

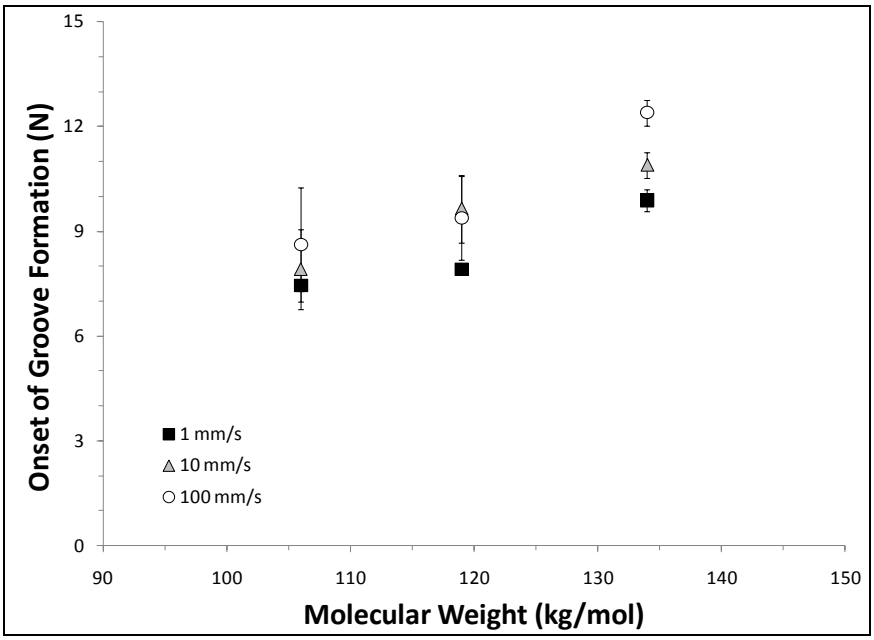

Figure 5.6 Critical load for the onset of groove formation for SAN model systems as a function of molecular weight.

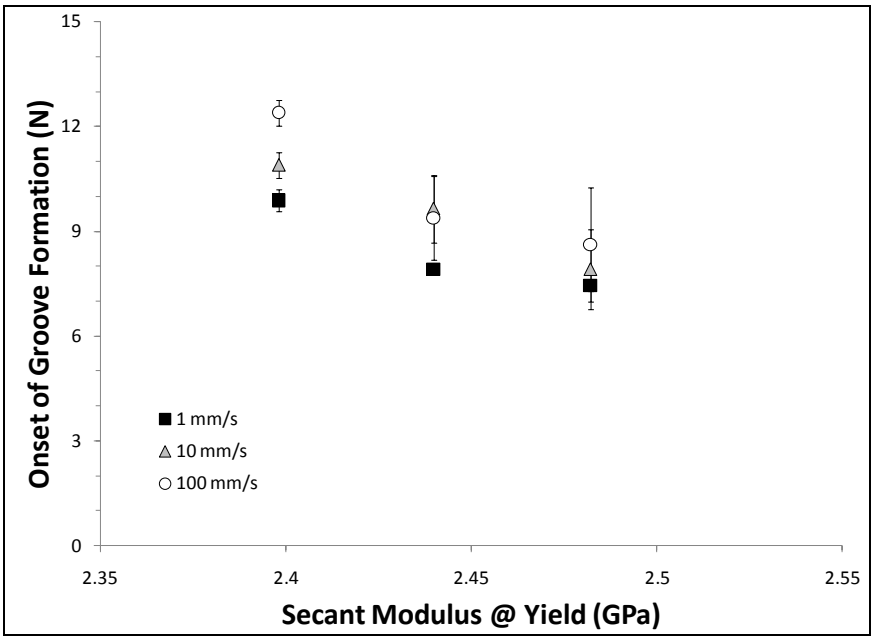

Figure 5.7 Critical load for the onset of groove formation as a function of secant modulus at the compressive yield point for SAN model systems with varying molecular weight.

5.3.2.2 Periodic Micro-cracking

It was stated in Section 2 that the tensile stress associated with this feature can more or less be considered to be uniaxial in nature. The uniaxial tensile strength of the SAN model systems has been shown to be positively related to the MW in Figure 5.5 and Figure 5.8 shows that this is also the case for the onset of periodic micro-cracking. So it makes sense that increasing the uniaxial tensile strength of SAN will effectively delay the onset of periodic micro-cracking as shown in Figure 5.9. This was also observed in the AN content effect study, which suggests that increasing the uniaxial tensile strength of SAN can improve its resistance to surface brittle fracture in the form of periodic micro-cracks.

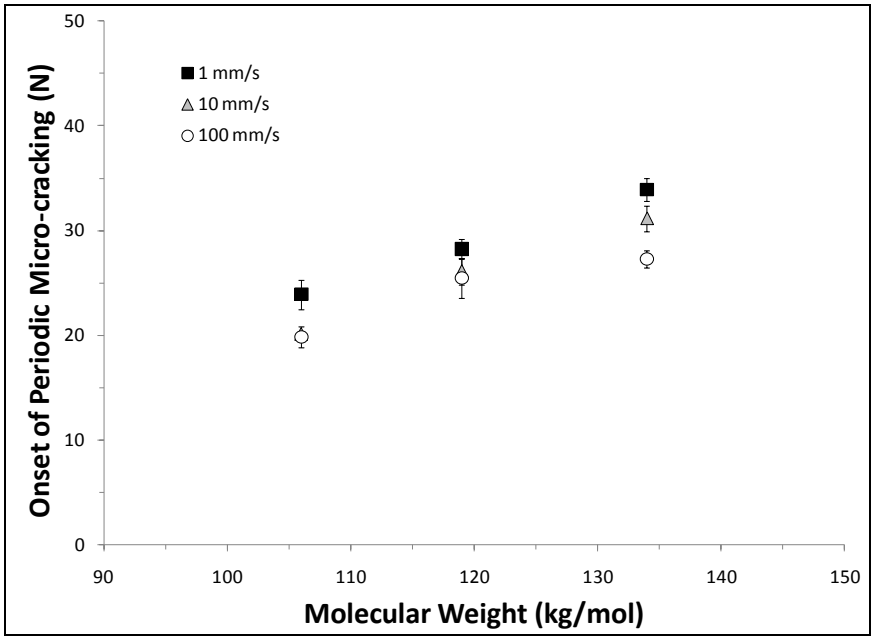

Figure 5.8 Critical load for the onset of periodic micro-cracking for SAN model systems as a function of molecular weight.

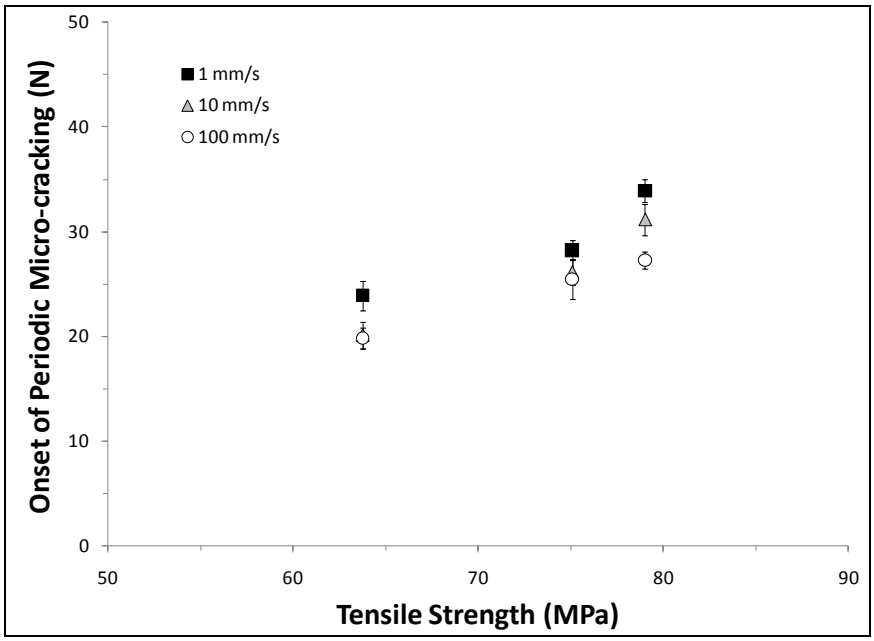

Figure 5.9 Critical load for the onset of periodic micro-cracking as a function of tensile strength for SAN model systems with varying molecular weight.

5.3.2.3 Plowing

Again, plowing is defined as ultimate material failure resulting from the development of multi-axial tensile stress component in front of the scratch tip. Figure 5.10 shows the critical load for the onset of plowing as a function of MW for the SAN model systems. It can be seen that increasing the MW can result in a slightly earlier onset of plowing. However, as the scratch speed increases, the MW effect diminishes. This is likely due to the fact that SAN is already quite brittle and becomes rate-insensitive at high speeds.

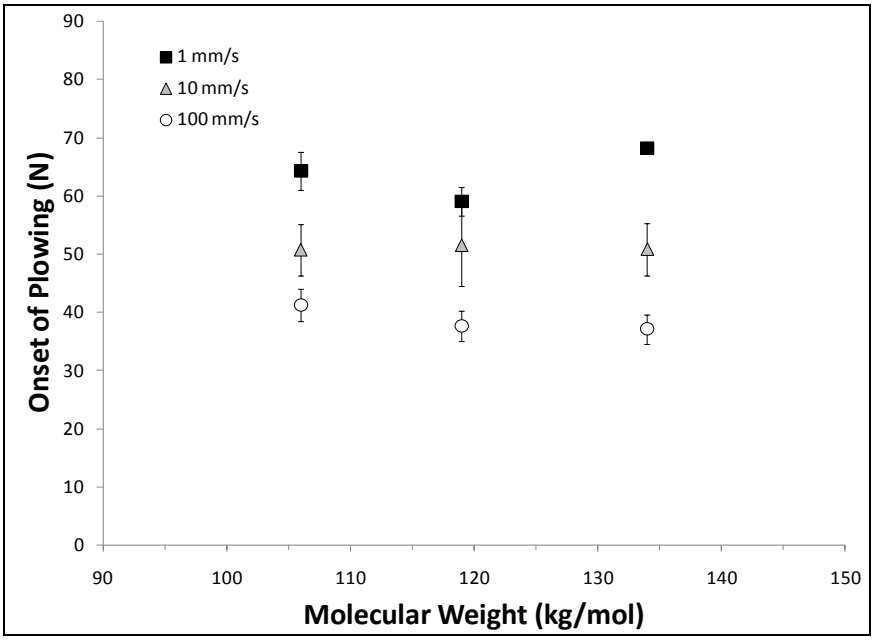

Figure 5.10 Critical load for the onset of plowing for SAN model systems as a function of molecular weight.

In Section 4, the uniaxial tensile strength was correlated with the onset of plowing and the result was fairly positive, but not as strong as the correlation with the

onset of periodic micro-cracking. This is also the case for the MW effect, as shown in Figure 5.11. Again, increasing the scratch speed seems to erase any effect seen from MW. Even though the onset of plowing deformation has been linked to tensile strength, it is recognized that the plowing deformation is in fact dominated by multi-axial stresses. Our previous stress analysis at the onset of plowing has indicated that the stress magnitude experienced by the material is at its highest level and is highly complex and multi-axial [66]. Therefore, it is possible that uniaxial tensile properties alone are not sufficient to address the physical nature of the plowing deformation mechanism.

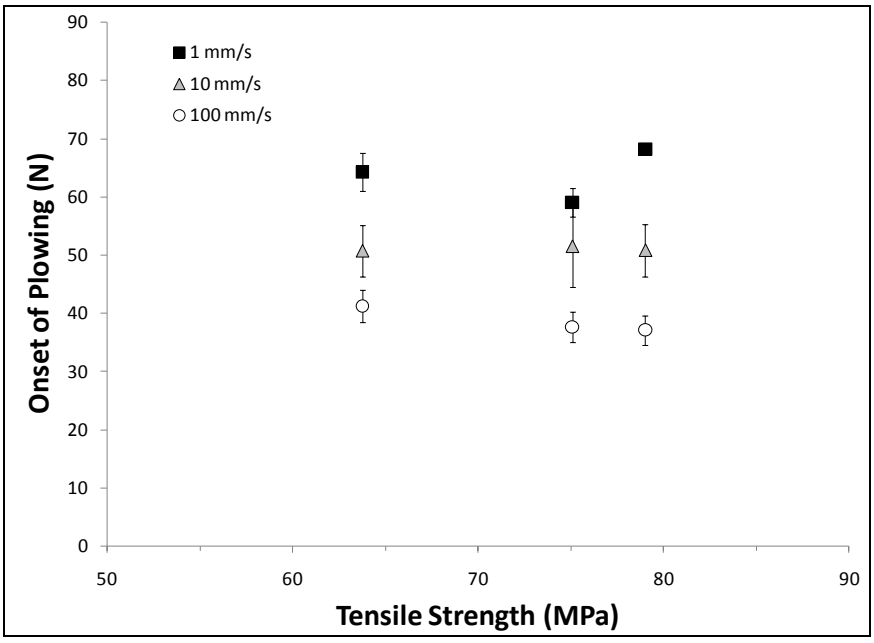

Figure 5.11 Critical load for the onset of plowing as a function of tensile strength for SAN model systems with varying molecular weight.

5.3.3 ScratchVisibility

The critical loads for the onset of scratch visibility as obtained with ASV® for all systems of the study at each speed and in each scanning orientation are shown in Figures 5.12 and 5.13. Example images after processing with ASV® are shown in Figure 5.3. In parallel orientation (Figure 5.12), a significant delay is observed in scratch visibility onset as the MW increases. For perpendicular orientation (Figure 5.13), the trend is similar to that seen in Figure 5.12, but the highest MW system appears to show a more delayed onset of visibility compared to the other two. Overall, the difference between the two orientations is small, but increasing the MW appears to have a generally favorable effect on enhancing the scratch visibility resistance of SAN.

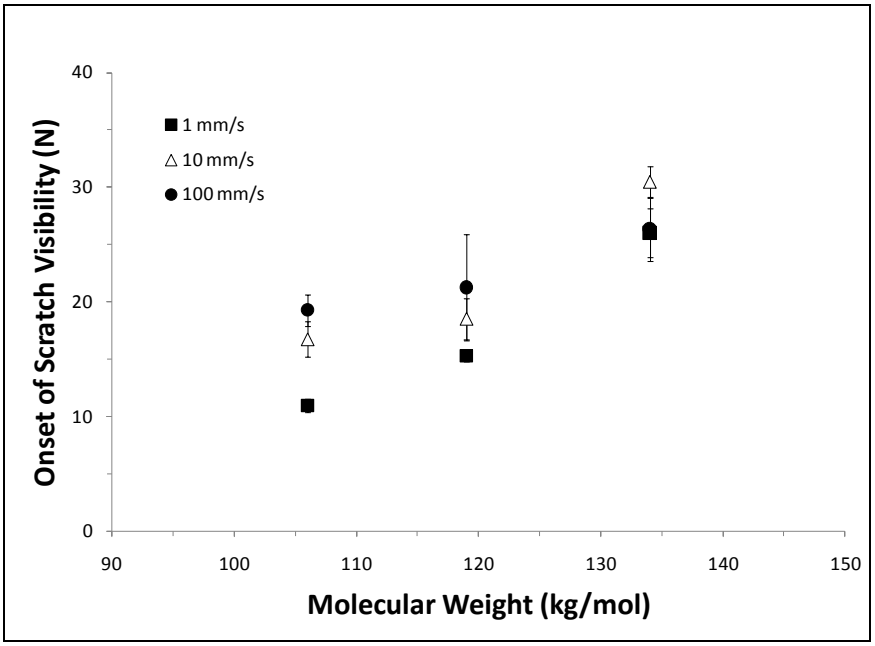

Figure 5.12 Critical load for the onset of visibility as obtained with ASV® software for SAN model systems in parallel illumination orientation.

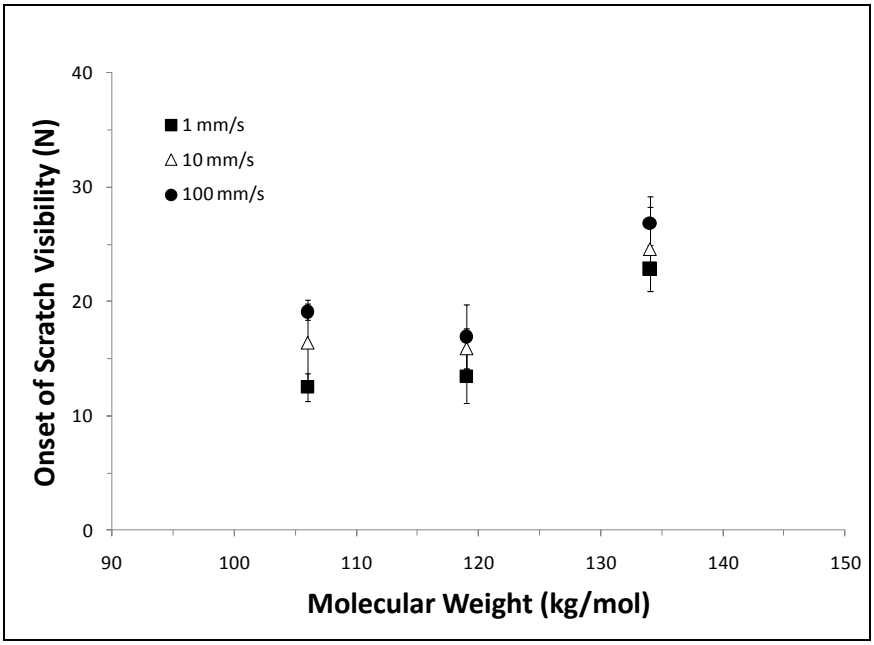

Figure 5.13 Critical load for the onset of visibility as obtained with ASV® software for SAN model systems in perpendicular illumination orientation.

5.3.4 Frictional Behavior

In a progressive load scratch test, the scratch depth continually increases with the applied load. As a result, the apparent coefficient of friction will progressively increase as a result of growing resistive force from the material in front of the scratch tip. The scratch coefficient of friction (SCOF) is defined as the ratio of the tangential and normal forces throughout the scratch. The SCOF vs. scratch distance curve can often give valuable clues to the location of transitions in scratch deformation mechanisms [12, 57]. For instance, when the onset of plowing occurs, the SCOF can change since the nature of deformation has changed from surface sliding to surface penetration and sub-surface material removal/machining.

The SCOF for the SAN systems of this study are shown at each speed as a function of scratch distance in Figures 5.14 – 5.16. At a scratch speed of 1 mm/s (Figure 5.14), the early portion of the SCOF curve shows some slight differentiation between the SAN systems. With the highest MW, SAN 27 C shows the lowest general SCOF curve prior to plowing. After the plowing onset, the SCOF for all the systems appears to converge. This effect has been observed in the scratch of PP and the wear of HDPE [40, 68, 78]. As the speed increases, however, the differentiation becomes less clear (Figures 5.15 and 5.16). This is likely due to the fact that polymers behave in a more brittle fashion as the testing speed increases. Since SAN is already a brittle material with a ductility of less than 3%, it makes sense that increasing the scratch speed would lead to a lower degree of differentiability. However, at low speeds, it can be said that increasing the MW can lead to a decrease in the SCOF.

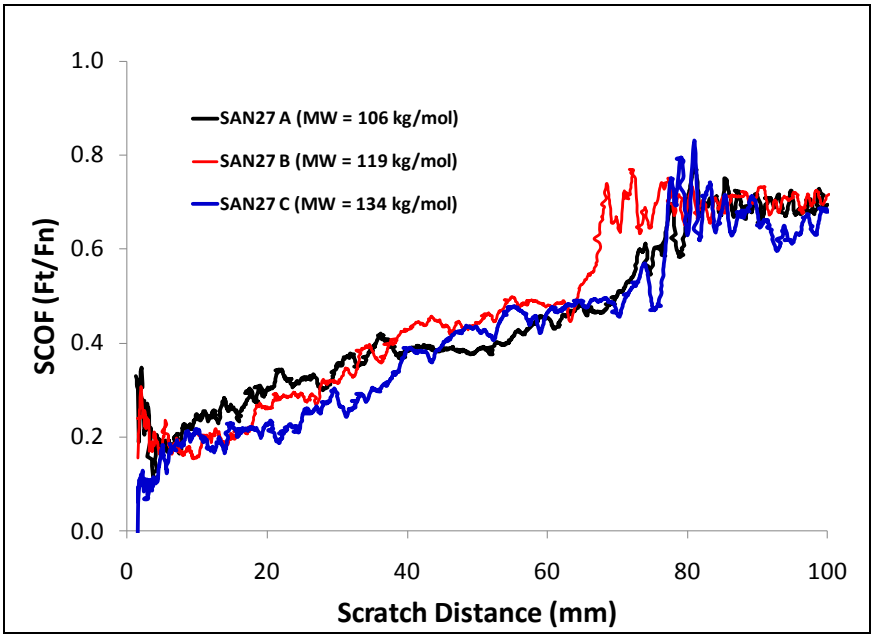

Figure 5.14 Scratch coefficient of friction as a function of scratch distance for SAN model systems with varying molecular weight. (Scratch speed = 1 mm/s)

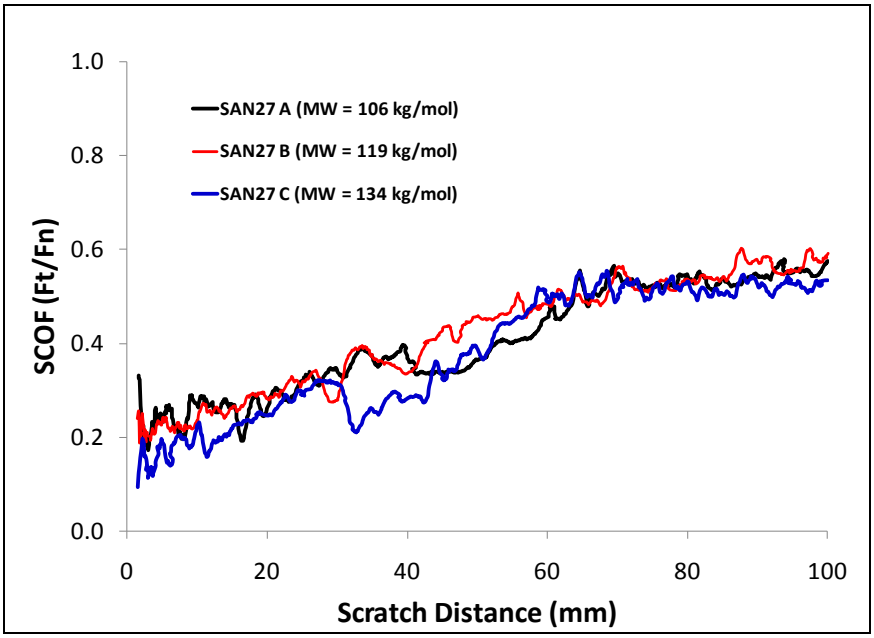

Figure 5.15 Scratch coefficient of friction as a function of scratch distance for SAN model systems with varying molecular weight. (Scratch speed = 10 mm/s)

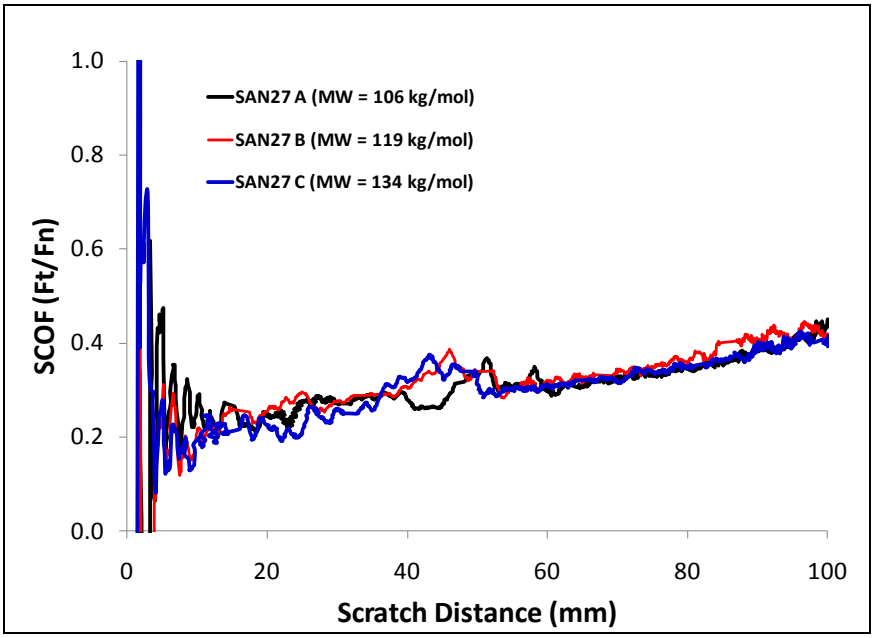

Figure 5.16 Scratch coefficient of friction as a function of scratch distance for SAN model systems with varying molecular weight. (Scratch speed = 100 mm/s)

6. EFFECT OF MOISTURE ABSORPTION ON SAN SCRATCH BEHAVIOR

It is important to consider the nature of the material surface when addressing scratch behavior. Even though a change of surface composition may have a small effect from the bulk standpoint, it could have a significant effect on surface properties. The AN phase of SAN contains a highly polar carbon-nitrogen triple bond (C≡N, dipole moment = 3.9 Debye), which can absorb environmental moisture and the amount to be absorbed is expected to increase with increasing AN content. The equilibrium bulk moisture absorption for SAN as reported in the literature is less than one percent [90]. However, since the absorption takes place initially within only a thin layer of the surface, the amount of moisture absorbed with respect to this surface layer is expected to have a strong influence on the scratch behavior. In this section, the effect of surface moisture absorption on the scratch behavior of SAN model systems of varying AN content is investigated.

6.1 Model SAN Systems

The physical properties of the SAN model systems are given in Table 6.1. It was verified that molecular weight imparts negligible influence on the moisture absorption behavior, so AN content is the focus of this investigation. Small coupons of the SAN systems with dimensions of 25.4 mm by 25.4 mm by 3 mm weighing ~1.5 g were used

to study the absorption behavior while large plaques with dimensions of 150 mm by 75 mm by 6 mm were used for the scratch study.

Table 6.1 Physical properties of SAN model systems for the moisture absorption study

	SAN 19	**SAN 27**	**SAN 35**
Acrylontrile Content (wt%)	19	27	35
Molecular Weight (kg/mol)	134	119	104
Polydispersity	4.1	4.3	3.7

6.2 Experimental Procedures

Plaques for the scratch study were annealed at 108 °C for 3 hours prior to any further treatment. All samples of the SAN systems were first dried overnight in an oven for 24 hours at 80 °C and a vacuum pressure of 30 mmHg. After drying, the small coupons were weighed using a digital scale. The samples were then placed in a sealed container with a dish holding potassium chloride salt and deionized water slurry. This allowed a controlled environment with an average relative humidity of ~70% and temperature of 23 °C. Over a period of ten days, the small coupons were periodically removed from the humid environment and weighed. The percentage weight change from the dry condition was used to monitor the moisture absorption behavior.

Following the analysis of the moisture absorption behavior with the small SAN coupons, the scratch plaques were subjected to exposure to the humid environment and periodically scratch tested over a ten-day period. A progressive normal load range of 1 – 90 N was applied at a scratch speed of 100 mm/s for a length of 100 mm. The tip was a

stainless steel ball with a diameter of 1 mm. The effect of moisture absorption was analyzed by obtaining the critical load for the onset of key deformation mechanisms for SAN as described in Section 4.

Scratch visibility was analyzed using ASV as described in Section 3 and high-resolution microscopic observation of the scratch damage morphology was carried out using a Keyence VK9700 VLSCM.

6.3 Results and Discussion

6.3.1 Moisture Absorption Behavior

The normalized weight gain for the SAN model systems is shown in Figure 6.1 as a function of days of exposure to the humid environment. It is easy to see that increasing the AN content increases the amount of water absorbed by the material and this is also reflected in Figure 6.2. The AN content effect is initially only minimal after one day of exposure, but then becomes more pronounced over the course of 3 days, after which the weight gain levels off. The trends presented in Figures 6.1 and 6.2 are rather intuitive. However, careful analysis suggests that the weight gain for all the systems occurred mostly within one day of moisture exposure.

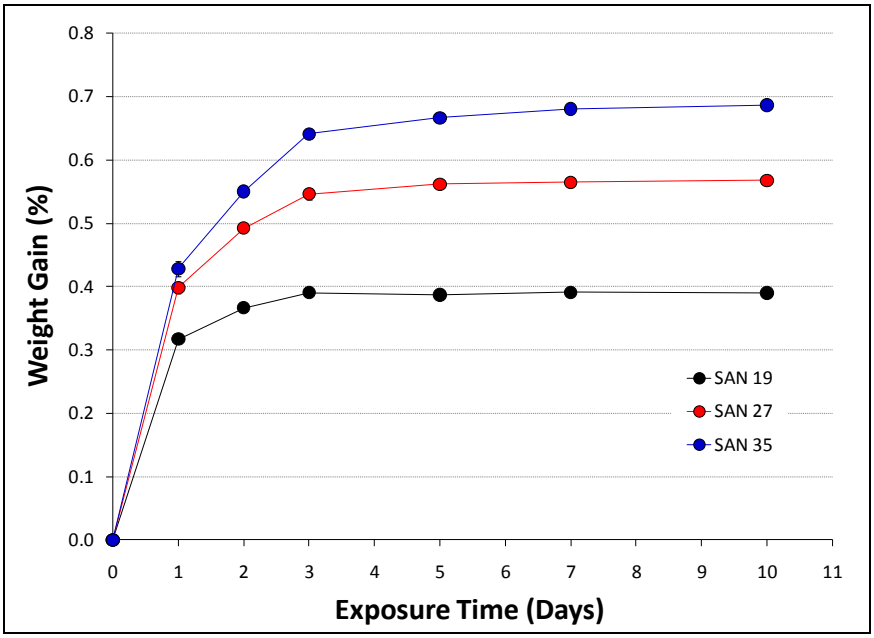

Figure 6.1 Percentage weight gain as a function of time exposed to a humid environment for SAN model systems. (R.H. = 70% at 23 °C)

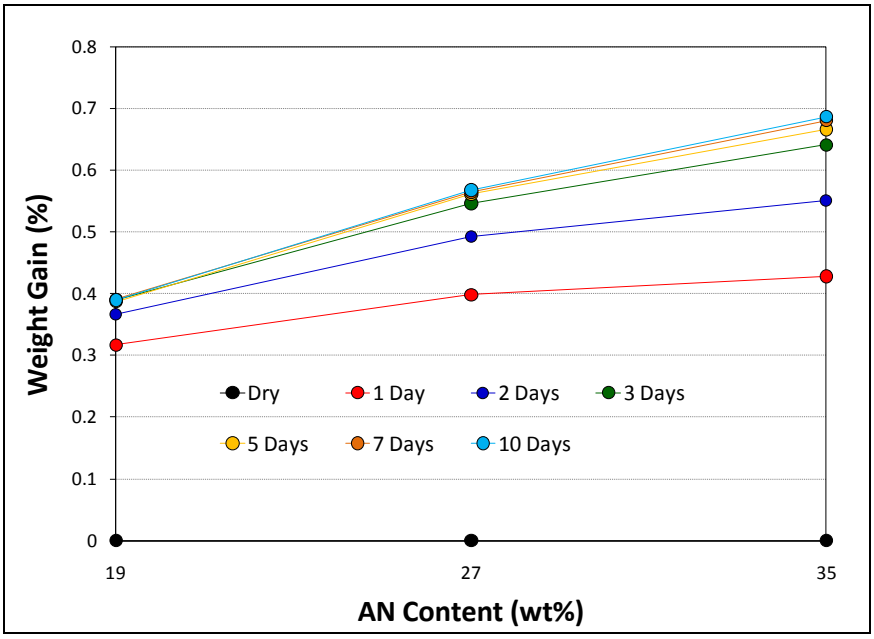

Figure 6.2 Percentage weight gain as a function of AN content for SAN systems in the moisture content study.

6.3.2 Diffusion Behavior

Initially, any moisture absorbed by the material is likely to be on the surface of the polymer. But as absorption continues, the moisture will diffuse into the polymer. The nature of the diffusion must first be understood before going further. To do so, the absorbed moisture at each time interval normalized against the saturation condition, M_t/M_{sat} was calculated using the following equation:

$$\frac{M_t}{M_{sat}} = \frac{w_t - w_{dry}}{w_{sat} - w_{dry}} \tag{6.1}$$

where w_t, w_{sat} and w_{dry} are the weight at time t, weight at saturation and dry weight, respectively. The weight at saturation was calculated by averaging the weight values for several measurements after saturation had been observed. A plot of M_t/M_{sat} versus the square root of exposure time, $t^{1/2}$, was constructed following the method of Shen and Springer [91] and is shown in Figure 6.3. The data points have been fit to an approximate solution to Fick's second law as evaluated by Shen and Springer [91]:

$$\frac{M_t}{M_{sat}} = 1 - \exp\left[-7.3\left(\frac{Dt}{l^2}\right)^{0.75}\right] \tag{6.2}$$

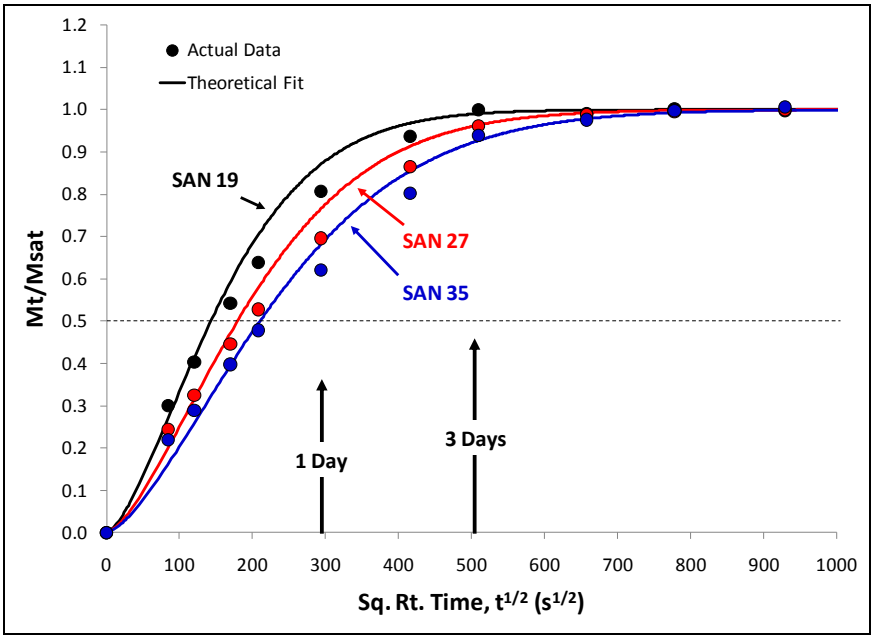

Figure 6.3 Moisture absorption plot for SAN model systems. Data points are fit to an approximate solution of Fick's 2nd law.

As Figure 6.3 suggests, the diffusion is of a reasonably Fickian nature. The diffusion coefficient, *D*, was approximated as in [92] by observing the time required to absorb have the saturation limit:

$$D = \frac{0.049 \cdot l^2}{t_{1/2}} \tag{6.3}$$

The diffusion coefficients for each AN content level are given in Figure 6.4. These values are close to the value of 3.4×10^{-8} cm^2/s reported by Bruder and Haese for SAN containing 28 wt% AN exposed to 50% R.H. at 23 °C [93]. From Figure 6.4, it can be concluded that increasing the AN content lowers the diffusivity. Given a unit volume, if there are more AN groups within that unit volume, a longer time will be required to reach saturation, resulting in a lower diffusivity.

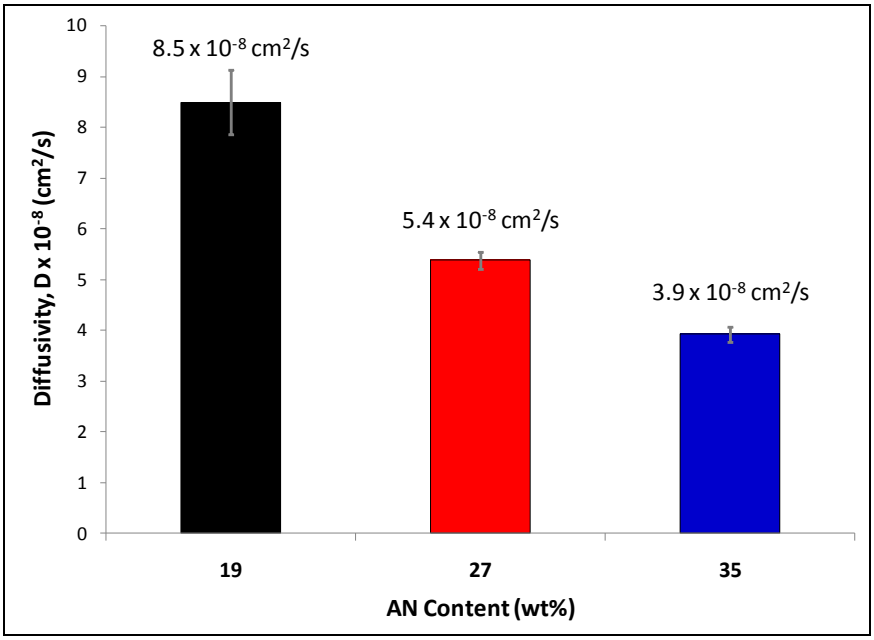

Figure 6.4 Diffusion coefficients for SAN model systems.

6.3.3 Scratch Behavior

The absorbed moisture is more than likely on the surface or contained within only a very thin layer of the sub-surface. As a result, the absorbed surface moisture is expected to affect the scratch behavior of SAN significantly. Indeed, upon scratching, the scratch behaviors of the moisture exposed model SAN systems appear quite complex, as shown in Figures 6.5 – 6.7. It is readily evident from the visual results that there is a drastic change in the scratch behavior during the first three days of moisture exposure. That is, the scratch resistance appears to deteriorate with moisture absorption in the first three days and then begins to improve afterwards.

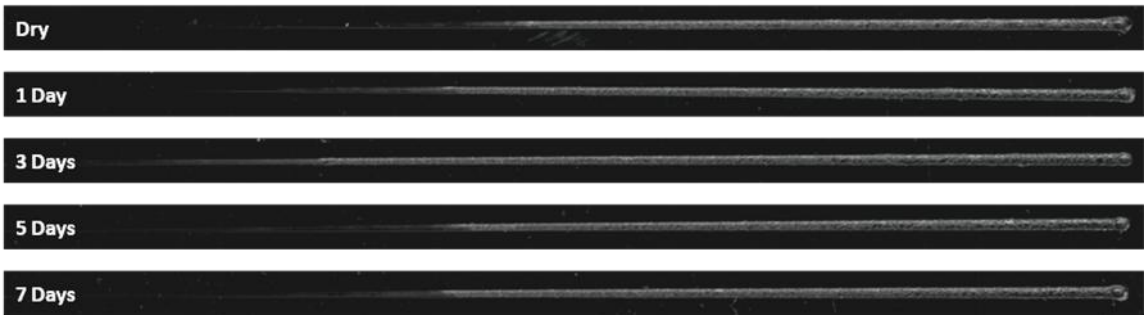

Figure 6.5 Digitally scanned images of SAN 19 periodically scratch tested after being exposed to a humid environment. (Resolution = 300 dpi)

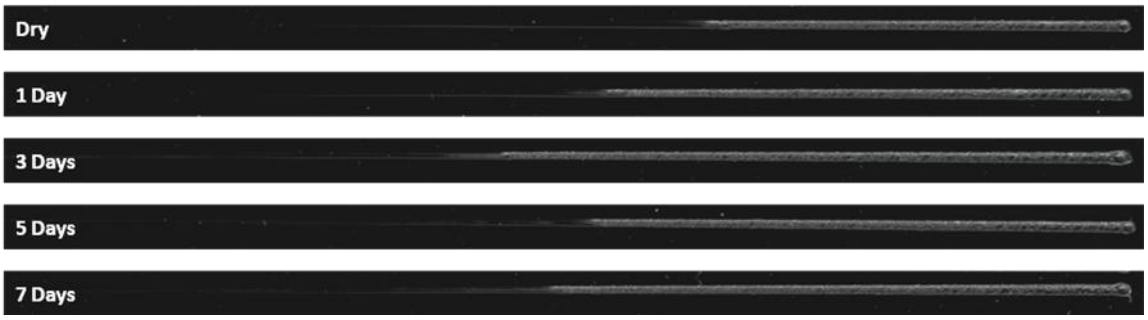

Figure 6.6 Digitally scanned images of SAN 27 periodically scratch tested after being exposed to a humid environment. (Resolution = 300 dpi)

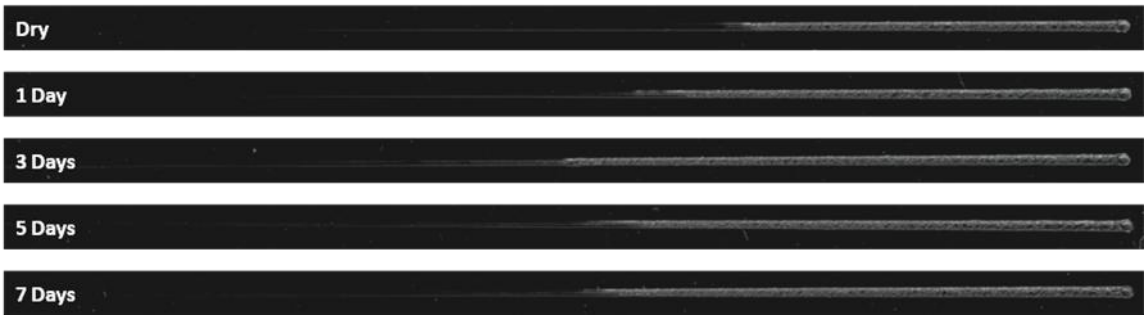

Figure 6.7 Digitally scanned images of SAN 35 periodically scratch tested after being exposed to a humid environment. (Resolution = 300 dpi)

This unusual behavior is most likely due to the fact that water molecules are first diffused into the sub-surface of the polymer, introducing a plasticizing effect which weakens the SAN and reduces its modulus and strength on the surface. Then, after saturation is reached, the water molecules form clusters on the surface which provides lubrication and improves the scratch performance slightly.

Further evidence is shown by examining the key deformation mechanisms for the SAN model systems. For scratch groove formation, the deformation was essentially instantaneous after three days exposure, so no effective differentiation could be made between the systems under these conditions. However, Figures 6.8 – 6.11 show that the other key scratch deformation mechanisms (scratch visibility, periodic micro-cracking and plowing) all follow a similar trend. There is an initial degradation in the scratch resistance up to the three day mark, followed by a slight recovery, although the behavior is most apparent in SAN 19.

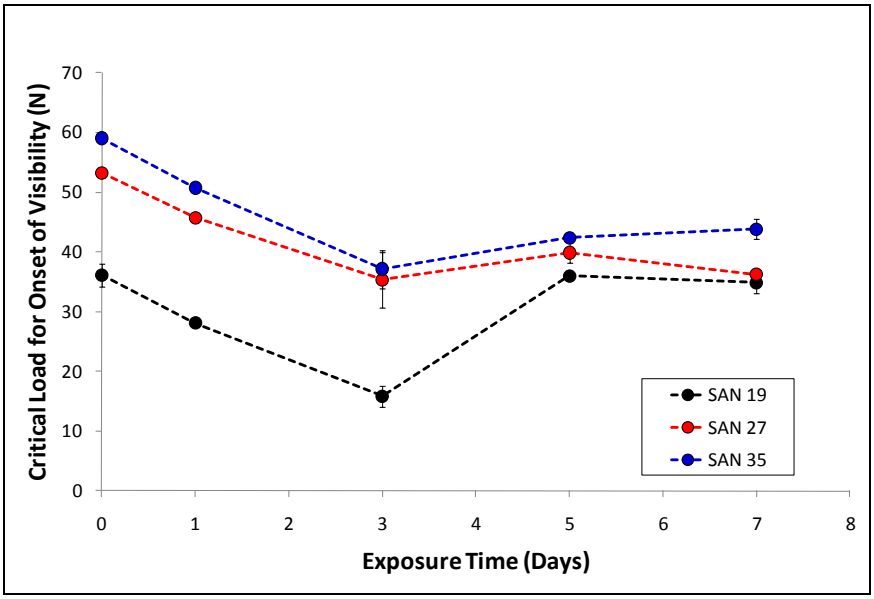

Figure 6.8 Critical load for the onset of visibility in parallel illumination orientation for SAN model systems as a function of exposure time.

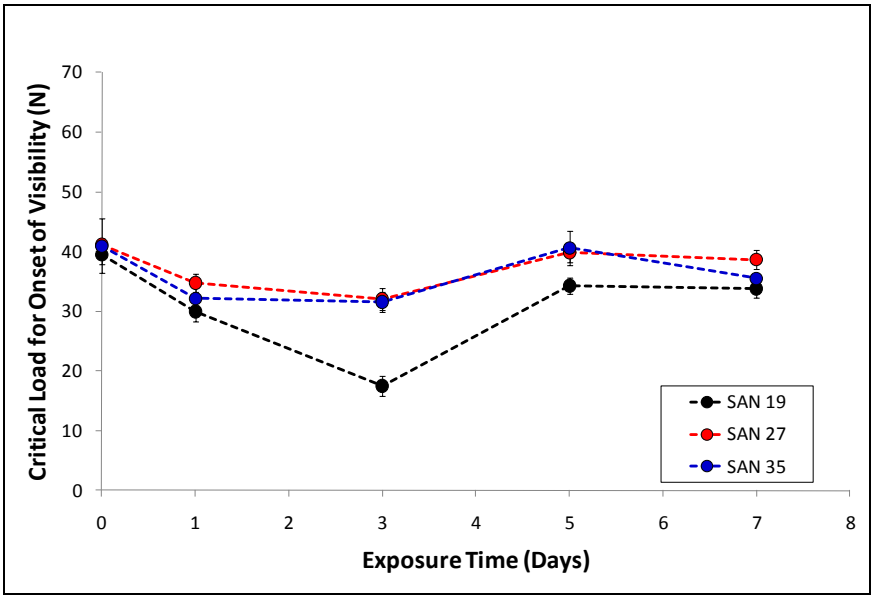

Figure 6.9 Critical load for the onset of visibility in perpendicular illumination orientation for SAN model systems as a function of exposure time.

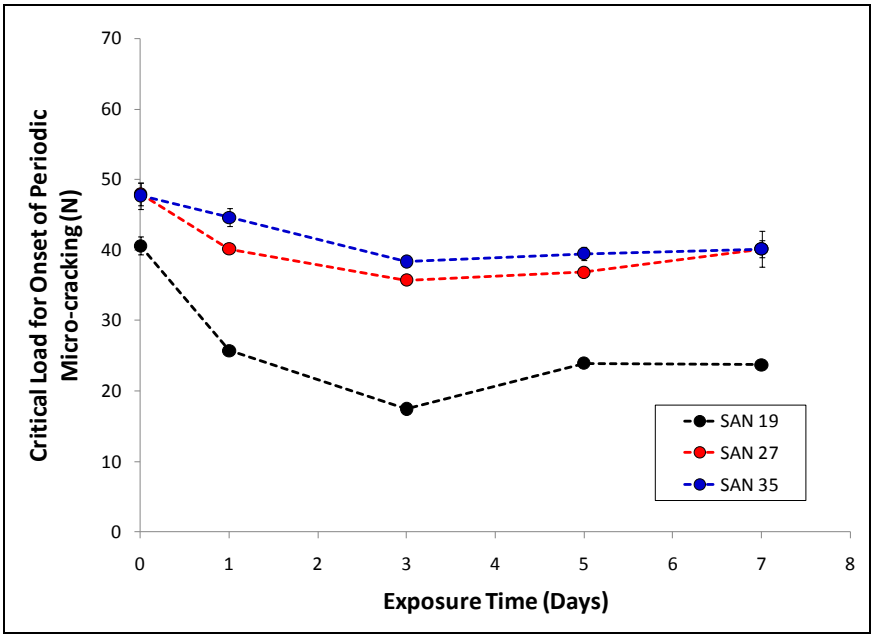

Figure 6.10 Critical load for the onset of periodic micro-cracking for SAN model systems as a function of exposure time.

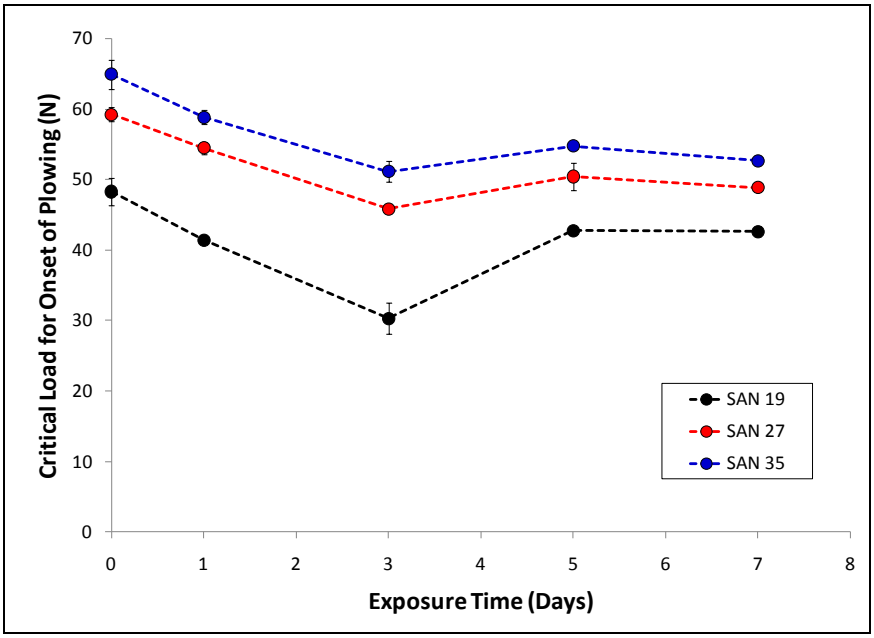

Figure 6.11 Critical load for the onset of plowing for SAN model systems as a function of exposure time.

The exact reason why there is such a prominent effect observed in SAN 19 is not currently known. It is proposed that due to its relatively low AN content, upon plasticization, the material behavior approaches that of polystyrene, which is known to have poor scratch resistance compared to most polymers. Then, after saturation is reached, the surface is lubricated and the resistance improves rather substantially.

The scratch coefficient of friction (SCOF) is a measure of the ratio of the scratch-induced tangential force and applied normal load. The surface lubrication claim is supported by the curves in Figures 6.12 – 6.14. The SCOF in the initial portion of the scratch displays a similar trend to the other key deformation mechanisms. It is highest at the three day mark and then becomes lower as exposure continues. It is known that a lower SCOF is associated with good scratch resistance [37, 63, 64]. Therefore, since it is suspected that the absorbed moisture is at the surface after saturation, the supposed lubrication effect is highly likely. Also, the spike later in the SCOF curve corresponds to the onset of plowing and the location of these spikes follows the similar trend of degradation followed by recovery.

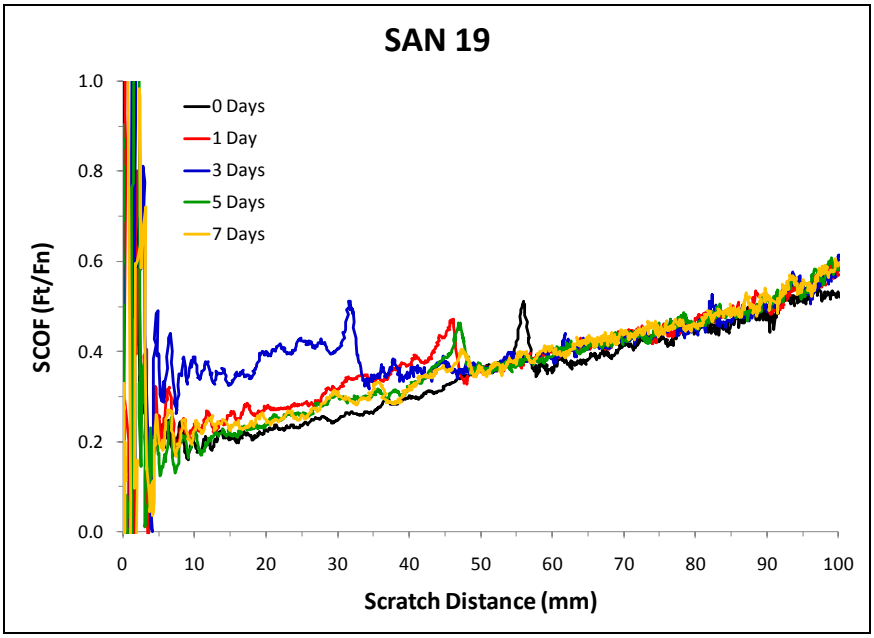

Figure 6.12 Scratch coefficient of friction as a function of scratch distance for SAN 19.

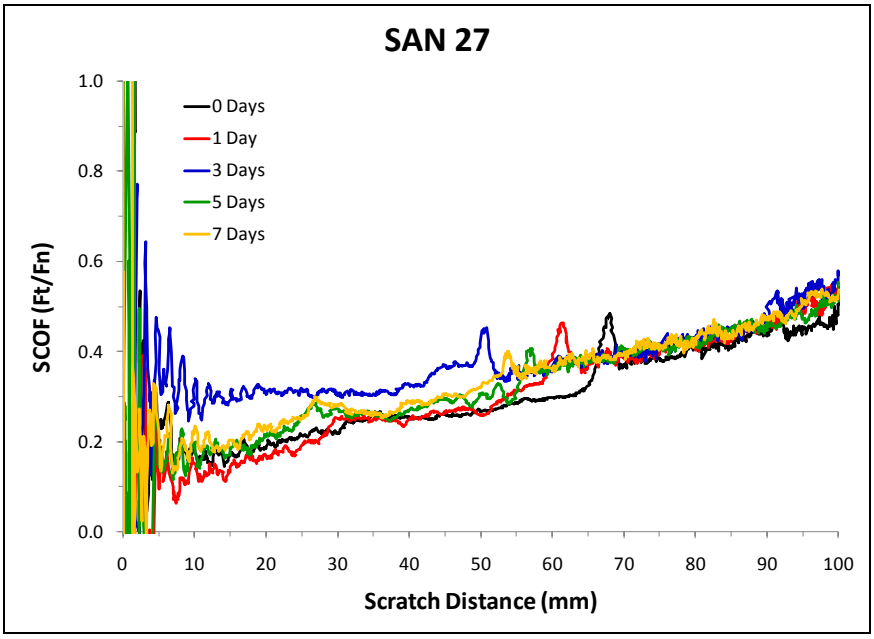

Figure 6.13 Scratch coefficient of friction as a function of scratch distance for SAN 27.

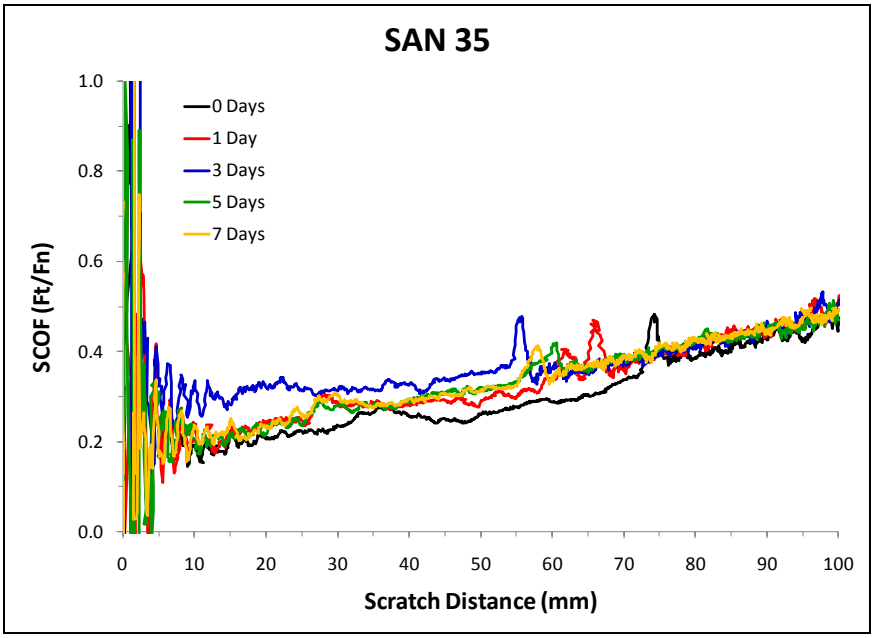

Figure 6.14 Scratch coefficient of friction as a function of scratch distance for SAN 35.

The bulk mechanical properties of SAN are not expected to change much as a result of absorbed moisture. It is assumed, however, that what moisture is absorbed is contained within a layer of the surface that is encountered by the scratch tip. Initially, before any moisture is absorbed, the SAN surface is rich in styrene when the AN content is below 50 wt% [94]. The absorption process could possibly be changing the nature of the SAN surface. It was stated that the initially absorbed moisture imparts plasticization. When this occurs in a polymer, the chains gain more mobility. Thus, at a certain level of absorbed moisture, a "flipping" mechanism could occur where the AN and styrene groups of the SAN chains at the surface swap places. This will ultimately result in a higher concentration of AN groups on the surface. Then, the water molecules can begin to cluster together provide surface lubrication.

In order to better understand how the absorbed moisture is influencing the SAN model systems on a molecular level, analysis must be undertaken with care and a high enough sensitivity to capture the changes in the molecular behavior. FTIR-ATR could provide a means to monitor any possible interaction of the AN groups with the water molecules. The level of molecular mobility as a function of moisture exposure could possibly be addressed using solid-state NMR. Also, changes in surface energy could be studied by contact angle measurements using an appropriate liquid medium. Nonetheless, these results show how important it is to consider the surface behavior of a material apart from its bulk behavior. Even though some factors may have a small effect from the bulk standpoint, those same factors could have a significant effect on the surface behavior.

7. CONCLUSIONS AND CONSIDERATIONS FOR FUTURE RESEARCH

7.1 Summary and Conclusions

The research effort in this dissertation was undertaken in order to gain fundamental understanding of polymer scratch behavior with regards to the relationship between mechanical properties and scratch deformation as well as scratch visibility. The focuses of the overall study were as follows:

1. Application of the software package ASV® to compare the resistance to scratch visibility of homopolymer polypropylene (PP) and polyvinylchloride (PVC) and gain insight regarding the relationship between scratch induced deformation and visibility.
2. Investigation of the effect of acrylonitrile (AN) content, which affects the mechanical properties of SAN, on the scratch behavior of SAN random copolymers with regards to mechanistic deformation and scratch visibility.
3. Study of the influence of molecular weight (MW) on the scratch behavior of the SAN model systems in a similar manner as the AN content effect study.
4. Investigation of the effect of absorbed surface moisture on SAN scratch behavior.

By using analysis criteria based on the physiology of the average human eye, ASV® has been shown to be a powerful tool to automatically analyze scratch visibility

in an objective and unbiased fashion. Upon analyzing the physical deformation related to scratch visibility, it was realized that two factors influence the onset of scratch visibility: changes in surface roughness and changes of scratch profile topology. Each deformation feature must reach a critical level in order to induce scratch visibility based on the physiological criteria. The orientation of the scratch direction with respect to an illumination source will govern which near surface deformation feature will influence visibility assessment. When the illumination orientation is perpendicular to the scratch direction, the topology of the scratch profile will have a dominant influence. In a parallel orientation, the roughness of the groove will dominate. The effectiveness of this approach was shown by validating the notion that PVC exhibits superior scratch visibility resistance compared to that of PP as it relates to scratch-induced deformation.

A fundamental approach to understanding polymer scratch behavior was carried out by applying the ASTM/ISO standard progressive load scratch test to a set of model SAN random copolymers with varying AN content and MW. Key scratch deformation mechanisms were identified as scratch groove formation, scratch visibility, periodic micro-cracking and plowing. Using a prior knowledge base founded upon mechanics and numerical simulation, correlations have been established between the compressive properties of the material and the scratch deformation mechanisms. Scratch groove formation can be linked to the secant modulus at the compressive yield point. A strong relationship between the uni-axial tensile strength and the onset of periodic micro-cracking was established, but the stress field for plowing is highly complex and it is

likely that uni-axial tensile properties are not sufficient to explain this deformation mechanism.

Specifically, it was realized that increasing the AN content and/or MW of the SAN copolymer results in enhanced scratch resistance with regards to all of the key deformation mechanisms. Increasing the AN content or MW lowers the secant modulus up to the compressive yield point which results in an increased contact area since variations in AN content and MW in the scope of this research do not alter the compressive yield stress values of SAN much. This will allow for a lower applied compressive stress and thus delay the onset of scratch groove formation. The tensile strength of the SAN systems increases with AN and MW and the onset of periodic micro-cracking and plowing is delayed in turn. With regards to scratch visibility, it was found that increasing the AN content or MW appears to impart an improvement in the resistance to the deformation mechanisms that induce visibility. Additionally, the frictional behavior of the material is improved somewhat as a result of AN content or MW increase. Increasing the scratch speed serves to increase brittleness of SAN, which is already inherently brittle. Therefore, scratch-induced deformation forms earlier.

Noting that the AN side group of the SAN backbone is highly polar, it was worth considering how absorbed surface moisture could affect the scratch behavior of the SAN model systems. The SAN model systems were exposed to a humid environment and periodically scratch tested according to the ASTM/ISO standard. Initially, the scratch resistance as it relates to the key deformation mechanisms degrades and is more than likely due to a surface plasticization effect from the absorbed moisture. However, after

three days exposure, the absorbed surface moisture acts as a lubricant and the scratch resistance begins to improve. This was evidenced by the fact that the friction behavior of the model systems was worst at three days of moisture exposure, but then showed improvement thereafter. Even though the bulk equilibrium moisture absorbance of SAN is less than one percent, the presence of moisture on the sample surface has a significant impact on the scratch performance.

7.2 Considerations for Future Research

Even though the findings presented in this dissertation are of significance in understanding the fundamental nature of polymer scratch behavior, there are still many factors that should be addressed to further our knowledge in better designing of scratch resistant polymers.

7.2.1 Mechanistic Understanding of Scratch Behavior

The main motivation for the work presented in this dissertation was the knowledge base gained from prior work completed by Jiang et al [63, 65, 66]. The parametric numerical simulation study was an important step in learning which mechanical properties influenced scratch behavior the most. The numerical simulation work furthered the understanding of the highly complex multi-axial stress field encountered during a scratch. Finally, the experimental categorization of scratch-induced deformation based on the strength and ductility of several polymers provided valuable foresight as to the relationship between mechanical behavior and scratch behavior.

Even though the findings of this dissertation work provide a degree of experimental corroboration for the numerical simulation, it is extremely important to realize that these findings only pertain to the type of polymer described herein; but more specifically, polymers that behavior linear-elastically in tension. All polymers exhibit post-yielding effects under compression (strain-softening, strain-hardening), but many polymers exhibit post-yielding in tension, as well. In tension, polystyrene (PS) is well known to be quite brittle in tension while polycarbonate (PC) is very ductile and shows distinct regions of strain-softening and hardening. Since the tensile properties of the material have been shown to influence the scratch behavior, it is expected that the scratch behavior of PS compared to PC will be fundamentally different. Since both polymers are amorphous and also since increasing MW has been linked to increasing tensile strength, PS and PC are good candidates for an experimental study to investigate the fundamental influences of differences in tensile stress-strain behavior on the scratch behavior.

However, it should also be noted that an in depth understanding of the behavior can only come from a combined experimental and numerical effort. A proper constitutive model that can encompass the entire spectrum of mechanical behavior (compressive and tensile) should be employed. Unfortunately, for now, no such constitutive model exists. It is suggested that efforts continue in hopes that a deeper understanding can be gained in this area.

7.2.2 Scratch Visibility Assessment

It was shown that the ASV® software is an excellent tool for automatically assessing scratch visibility resistance in an objective and unbiased fashion. This is indeed true, but so far, results have been the most consistent when the virgin surface is uniformly smooth. Often, polymer surfaces can naturally possess or can be manufactured with non-uniform surface textures or patterns that change the way that incident light interacts with the surface. This in turn affects the physical nature of scratch visibility. The difficulty lies in the fact that a computer cannot make judgments as a human can as to what surface features are associated with a scratch and what features are either involved with the surface texture or are anomalous (dust particles, bumps, etc.). Because of this, any digital "machine vision" method of assessment should only serve as a supplement to true human observations, not a substitute. Hopefully, with more work, this challenge can be overcome by developing a technology that can differentiate a visible scratch from a non-uniform background.

REFERENCES

[1] Scheirs J, Priddy DB. Modern Styrenic Polymers. San Francisco: John Wiley & Sons, Inc.; 2006.

[2] Kody RS, Martin DC. Polymer Engineering and Science 1996; 36: 298 – 304.

[3] Bertrand-Lambotte P, Loubet JL, Verpy C, Pavan S. Thin Solid Films 2001; 398 – 399: 306 – 312.

[4] Bertrand-Lambotte P, Loubet JL, Verpy C, Pavan S. Thin Solid Films 2002; 420 – 421: 281 – 286.

[5] Blees MH, Winkelman GB, Balkenende AR, den Toonder JMJ. Thin Solid Films 2000; 359: 1 – 13.

[6] Bull SJ, Rickerby DS. Surface and Coatings Technology 1990; 42: 149 – 164.

[7] Bull SJ. Surface and Coatings Technology 1991; 50: 25 – 32.

[8] Consiglio R, Randall NX, Ballaton B, von Stebut J. Thin Solid Films 1998; 332: 151 – 156.

[9] Flosbach C, Schubert W. Progress in Organic Coatings 2001; 43: 123 – 130.

[10] Li JCM. Materials Science and Engineering A – Structures 2001; A317: 197 – 203.

[11] Wong JSS, Sue HJ, Zeng KY, Li RKY, Mai YW. Acta Materialia 2004; 52: 431 – 443.

[12] Wong M, Lim GT, Moyse A, Reddy JN, Sue HJ. Wear 2004; 256: 1214 – 1227.

[13] Guevin PR. Journal of Coating Technology 1995; 67: 61 – 65.

[14] Vingsbo O, Hogmark S. Wear 1984; 100: 489 – 502.

[15] Liang YN, Li SZ, Li DF, Li S. Wear 1996; 199: 66 – 73.

[16] Chanda A, Basu D. Dasgupta A, Chattopadhyay S, Mukhopadhyay AK. Journal of Materials Science Letters 1997; 16: 1647 – 1651.

[17] Krupicka A, Johansson M, Hult A. Progress in Organic Coatings 2003; 46: 32 – 48.

[18] Chu J, Rumao L, Coleman B. Polymer Engineering and Science 1998; 38: 1906 – 1914.

[19] Chu J, Xiang C, Sue HJ, Hollis RD. Polymer Engineering and Science 2000; 40: 944 – 955.

[20] Hogberg H. Modern Plastics 1955; 33: 150, 152, 157 and 259.

[21] Briscoe BJ, Smith AC. Nature 1979; 278: 725 – 726.

[22] Briscoe BJ, Stolarski TA. American Chemical Society Symposium Series 1985; 287: 303 – 313.

[23] Briscoe BJ, Evans PD. Composite Science Technology 1989; 34: 73 – 90.

[24] Briscoe BJ. Scripta Mettalurgica Materialia 1990; 24: 839 – 844.

[25] Briscoe BJ, Biswas SK, Sinha SK, Panesar SS. Tribology International 1993; 26: 183 - 193.

[26] Briscoe BJ, Pelillo E, Sinha SK. Polymer Engineering and Science 1996; 36: 2996 – 3005.

[27] Briscoe BJ, Pelillo E, Sinha SK. Polymer International 1997; 43: 359 – 367.

[28] Briscoe BJ, Sinha SK. Tribology International 1997; 30: 475 – 482.

[29] Briscoe BJ, Evans PD, Pelillo E, Sinha SK. Wear 1996; 200: 137 – 147.

[30] Briscoe BJ. Tribology International 1998; 31: 121 – 126.

[31] Briscoe BJ, Chateuaminois A, Lindley TC, Parsonage D. Tribology International 1998; 31: 701 – 711.

[32] Briscoe BJ, Pelillo E, Ragazzi F, Sinha SK. Polymer 1998; 39: 2161 – 2168.

[33] Briscoe BJ, Delfino A, Pelillo E. Wear 1999; 229: 319 – 328.

[34] Briscoe BJ, Chateauminois A. Tribology International 2002; 35: 245 – 254.

[35] Briscoe BJ, Sinha SK. Materialwissenschaft und Werkstofftechnik 2003; 34: 989 – 1002.

[36] Britz D, Ryntz RA, Jardret V, Yaneff PV. JCT Coatings Tech 2006; 3: 40 – 46.

[37] Browning R, Lim GT, Moyse A, Sun LY, Sue HJ. Polymer Engineering and Science 2006; 46: 601 – 608.

[38] Browning RL, Lim GT, Moyse A, Sue HJ, Chen H, Earls JD. Surface Coatings and Technology 2006; 201: 2970 – 2976.

[39] Dasari A, Duncan SJ, Misra RDK. Materials Science and Technology 2002; 18: 1227 – 1234.

[40] Dasari A, Duncan SJ, Misra RDK Materials Science and Technology 2003; 19: 239 – 243.

[41] Dasari A, Rohrmann J, Misra RDK. Materials Science and Technology 2003; 19: 1298 – 1308.

[42] Dasari A, Rohrmann J, Misra RDK. Materials Science and Technology 2003; 19: 1458 – 1466.

[43] Dasari A, Misra RDK, Rohrmann J. Polymer Engineering and Science 2004; 44: 1738 – 1748.

[44] Dasari A, Rohrmann J, Misra RDK. Materials Science and Engineering A – Structures 2004; 364: 357 – 369.

[45] Hadal R, Dasari A, Rohrmann J, Misra RDK. Materials Science and Engineering A – Structures 2004; 380: 326 – 339.

[46] Hadal R, Misra RDK. Materials Science and Engineering A – Structures 2004; 398: 252 – 261.

[47] Hadal R, Yuan Q, Jog JP, Misra RDK. Materials Science and Engineering A – Structures 2006; 418: 268 – 281.

[48] Jardret V, Ryntz R. JCT Research 2005; 2: 591 – 598.

[49] Jones FN, Shen W, Smith SM, Huange ZH, Ryntz RA. Progress in Organic Coatings 1998; 34: 119 – 129.

[50] Lim GT, Reddy JN, Sue HJ. Stimuli-Responsive Polymeric Films and Coatings 2005; 912: 155 – 180.

[51] Lim GT, Wong MH, Reddy JN, Sue HJ. JCT Research 2005; 2:361 – 369.

[52] Mi L, Ling H, Shen WD, Ryntz R, Wichterman B, Scholten A. JCT Research 2006; 3: 249 – 255.

[53] Misra RDK, Hadal R, Duncan SJ. Acta Materialia 2004; 52: 4363 – 4376.

[54] Ryntz RA, Abell BD, Pollano GM, Nguyen LH, Shen WC. Journal of Coatings Technology 2000; 72: 47 – 53.

[55] Ryntz RA, Britz D. Journal of Coatings Technology 2002; 74: 77 – 81.

[56] Sinha SK. Tribology International 2006; 39: 61-190.

[57] Wong M, Moyse A, Lee F, Sue HJ. Journal of Materials Science 2004; 39: 3293 – 3308.

[58] Xiang C, Sue HJ, Chu J, Coleman B. Journal of Polymer Science – Polymer Physics 2001; 39: 47 – 59.

[59] Xiang C, Sue HJ, Chu J, Masuda K. Polymer Engineering and Science 2001; 41: 23 – 31.

[60] ASTM International, ASTM D7027–05; 2005.

[61] International Organization for Standardization, ISO 19252:2008; 2008.

[62] Browning R, Jiang H, Moyse A, Sue HJ, Iseki Y, Ohtani K, Ijichi Y. Journal of Materials Science 2008; 43: 1357 – 1365.

[63] Jiang H, Lim GT, Reddy JN, Whitcomb JD, Sue HJ. Journal of Polymer Science B: Polymer Physics 2007; 45: 1435 – 1447.

[64] Jiang H, Browning R, Fincher J, Gasbarro A, Jones S, Sue HJ. Applied Surface Science 2008; 254: 4494 – 4499.

[65] Jiang H, Browning R, Sue HJ. Polymer 2009; 50: 4056 – 4065.

[66] Jiang H, Browning R, Whitcomb JD, Ito M, Shimouse M, Chang TA, Sue HJ. Tribology Letters 2010; 37: 159 – 167.

[67] Jiang H, Browning R, Hossain MM, Sue HJ, Fujiwara M. Applied Surface Science 2010; doi:10.1016/j.apsusc.2010.04.011.

[68] Moghbelli E, Browning R, Boo WJ, Hahn SF, Feick LJE, Sue HJ. Tribology International 2008; 41: 425 – 433.

[69] Moghbelli E, Sun L, Jiang H, Boo WJ, Sue HJ. Polymer Engineering and Science 2009; 49: 483 – 490.

[70] Jardret V, Morel P. Progress in Organic Coatings 2003; 48: 322 – 331.

[71] Lafaye S, Gauthier C, Schirrer R. Wear 2008; 265: 664 – 673.

[72] Charrault E, Gauthier C, Marie P, Schirrer R. Journal of Polymer Science B: Polymer Physics 2008; 46: 1337 – 1347.

[73] Pelletier H, Gauthier C, Schirrer R. Materials Letters 2009; 63: 1671 – 1673.

[74] Pelletier H, Gauthier C, Schirrer R. Wear 2010; 268: 1157 – 1169.

[75] Mudaliar A, Yuan Q, Misra RDK. Polymer Engineering and Science 2006; 46: 1625 – 1634.

[76] Yuan Q, Ramisetti N, Misra RDK. Acta Materialia 2008; 56: 2089 – 2100.

[77] Dasari A, Yu ZZ, Mai YW. Materials Science and Engineering R 2009; 63: 31 – 80.

[78] Guermazi N, Elleuch K, Ayedi HF, Zahouani H, Kapsa, P. Materials Science and Engineering A 2008; 492: 400 – 406.

[79] McNie C, Barton DC, Stone MH, Fisher J. Proceedings of the Institution of Mechanical Engineers 1998; 212: 49 – 56.

[80] Mcnie CM, Barton DC, Ingham E, Tipper JL, Fisher J, Stone MH. Journal of Materials Science: Materials in Medicine 2000; 11: 163 – 174.

[81] Kanaga Karuppiah KS, Bruck AL, Sundararajan S, Zhiqun L. Materials Research Society Symposium Proceedings 2006; 977: 78 – 84.

[82] Kanaga Karuppiah KS, Bruck AL, Sundararajan S. ASME/STLE International Joint Tribology Conference Proceedings 2008; PART B: 953 – 955.

[83] Paul MC, Glennon LP, Baer TE, Brown TD. Journal of Biomechanical Engineering 2008; 130: 061019-1 - 061019-10.

[84] DesJardins JD, Burnikel B, LaBerge M. Wear 2008; 264: 245 – 256.

[85] Hutchings IM, Wang PZ, Parry GC. Surface Coatings and Technology 2003; 165: 186 – 193.

[86] Rangarajan P, Sinha M, Watkin V, Harding K, Sparks J. Polymer Engineering and Science 2003; 3: 749 – 758.

[87] Shin E, Hiltner A, Baer E. Journal of Applied Polymer Science 1993; 47: 245 - 267.

[88] Boyce MC, Arruda EM, Jayachandran R. Polymer Engineering and Science 1994; 34: 716 - 725.

[89] Haward RN, Young RJ. The Physics of Glassy Polymers. New York: Chapman and Hall; 1997.

[90] Smith WM. Vinyl Resins. New York: Reinhold Publishing Corporation; 1958.

[91] Shen CH, Springer GS. Journal of Composite Materials 1976; 10: 2 – 20.

[92] Hansen CM. Polymer Engineering and Science 1980; 20: 252 – 258.

[93] Bruder F, Haese W. Japanese Journal of Applied Physics 1999; 38: 1709 – 1710.

[94] Adão MHVC, Saramago BJV, Fernandes AC. Journal of Colloid and Interface Science 1999; 217: 94 – 106.

VITA

Name:	Robert Lee Browning
Address:	3123 TAMU College Station, TX 77843-3123
Email Address:	B_Squared02@yahoo.com
Education:	B.S., Chemical Engineering, Texas A&M University, 2004 M.S., Mechanical Engineering, Texas A&M University, 2006